Manuscript submitted to: Volume 2, Issue 2, 122-162.

AIMS Materials Science DOI: 10.3934/matersci.2015.2.122

Received date 27 March 2015, Accepted date 09 June 2015, Published date 16 June 2015

Review

Possibilities and Challenges of Scanning Hard X-ray Spectro-microscopy Techniques in Material Sciences

Andrea Somogyi * and Cristian Mocuta

Synchrotron Soleil, BP 48, Saint-Aubin, Gif sur Yvette, 91192, France

*** Correspondence:** Email: somogyi@synchrotron-soleil.fr.

Abstract: Scanning hard X-ray spectro-microscopic imaging opens unprecedented possibilities in the study of inhomogeneous samples at different length-scales. It gives insight into the spatial variation of the major and minor components, impurities and dopants of the sample, and their chemical and electronic states at micro- and nano-meter scales. Measuring, modelling and understanding novel properties of laterally confined structures are now attainable. The large penetration depth of hard X-rays (several keV to several 10 keV beam energy) makes the study of layered and buried structures possible also in *in situ* and *in operando* conditions. The combination of different X-ray analytical techniques complementary to scanning spectro-microscopy, such as X-ray diffraction, X-ray excited optical luminescence, secondary ion mass spectrometry (SIMS) and nano-SIMS, provides access to optical characteristics and strain and stress distributions. Complex sample environments (temperature, pressure, controlled atmosphere/vacuum, chemical environment) are also possible and were demonstrated, and allow as well the combination with other analysis techniques (Raman spectroscopy, infrared imaging, mechanical tensile devices, etc.) on precisely the very same area of the sample. The use of the coherence properties of X-rays from synchrotron sources is triggering emerging experimental imaging approaches with nanometer lateral resolution. New fast analytical possibilities pave the way towards statistically significant studies at multi-length-scales and three dimensional tomographic investigations. This paper gives an overview of these techniques and their recent achievements in the field of material sciences.

Keywords: scanning hard X-ray microscopy; spectro-microscopy; elemental distribution; chemical state; impurities; dopants; multi-technique imaging; local strain; lattice parameter; lensless microscopy

1. Introduction

Beyond ensemble averages, technologically important materials are often inhomogeneous on many different length scales; multiple phases, precipitates, voids, dislocation networks, grains, grain-boundaries and layered structures all affect materials behavior. Characterization with high spatial resolution and at multi length-scales is therefore crucial to understand the role of heterogeneities, local sample characteristics, their deviation and impact on the average sample characteristics and behavior, and also to tailor the material properties by adapted material engineering. Moreover, several scientific questions are to be answered when nanoscale is approached, in order to understand the novel properties of laterally confined structures. For these *in situ* investigations are necessary. For functionality studies in *in operando* conditions, see for ex. [1,2], or for successive investigations, the preservation of the specimen's integrity is a prerequisite.

Microscopy-like techniques are of great importance and undergo huge developments with the appearing of nano-sciences; they contributed in an undoubtable way to manufacture, optimize and understand such structures and consequently finely tune their properties. X-ray analysis methods are among these important and useful tools. Without questioning the interest and the advantages of using well established microscopy techniques, using X-rays, especially from synchrotron radiation sources has a number of advantages, such as high collimation, high temporal coherence, polarisation and continuous tunability, which makes X-ray microscopies an important complementary tool [e.g. 3]. The X-ray energy range is usually divided into two major energy domains, with somehow arbitrary energy limits; to the soft X-ray range ~100–2500 eV and the hard X-ray range (several keV to several 10 keV beam energy). In the last 20 years, synchrotron-based soft X-ray microscopy has emerged as a powerful technique for chemical microanalysis [e.g. 4,5,6,7] and has been successfully applied to important material science studies [e.g. 8,3] providing excellent quantitative elemental and chemical sensitivity. In this energy range the 1s core (K-edges) electrons of light elements or the 2p core electrons (L2,3 edges) of heavier elements can be studied typically by chemical imaging. If coupled to the polarization state of the photons, soft X-ray microscopy techniques can also characterize bond orientation and magnetic domain structure [6]. Excellent review papers are available covering the recent research in this energy domain [5,6,7].

In this paper we focus on hard X-ray based microscopy techniques, which does have a number of additional advantages: minimal sample preparation and damage, possibility of investigating up to several tens μm thick samples, access to buried surfaces and interfaces, quantitative sensitivity to trace elements, access to chemical environment (tuning to absorption edges), access to strain (at a level hardly achievable with other techniques), possibility to include specific sample environments for *in operando* studies. The disadvantages are to be put into balance: a heavier setup (mostly available at synchrotron sources), working in the reciprocal (Fourier transform) space in diffraction, sometimes less sensitivity to the very top/thin surfaces (compared, for example, to the electron microscopy or electron spectroscopy, though techniques like X-ray reflectivity or Grazing Incidence X-ray diffraction allow characterizing sub nm-thick layers). We think that hard X-ray microscopy should be considered as a complementary (noninvasive) technique with respect to other microscopy techniques, and giving access to complementary information, in order to have a more complete image of the overall sample properties.

If a relatively large, (sub)-mm sized X-ray is used, large areas of the samples will be investigated (be it with spectroscopic or diffraction methods). In a first approach, this is seen as an

advantage compared to local microscopy techniques as the measured average quantities are characteristic of the sample surface and volume exposed to the X-rays. Averaging over millimeter lateral sizes was and still is very difficult today using other approaches. Thus, part of X-ray investigations were mostly concentrating on analyzing large samples containing micro-/nano-structures composed of (almost) identical individual objects (or with low dispersions in the properties of the individual objects). The measured average property is thus attributed to the local property of a single structure (which is the average single object). Statistical information (e.g. average parameters and corresponding dispersion) can also be obtained. On the other hand, for numerous cases, e.g. multi-modal growth, complex samples (e.g. in microelectronics), the "average" object does not make sense anymore and the application of X-ray microscopy techniques providing micro-/nano-meter spatial resolution is becoming essential.

Full field X-ray microscopy provides information on the sample morphology (electron density). Its advantage is the possibility of obtaining fast 3 dimensional (3D) information down to sub-μm or even sub-100 nm spatial resolutions; by using either an X-ray objective (e.g. Fresnel Zone Plate lens) behind the sample or by projection microscopy (no optics behind the sample, and using a highly divergent beam) to obtain magnified images. Full field microscopy methods may also provide chemical information about the major (expected at least few percent concentrations) sample components [9,10] by measuring transmission imaging before and after their absorption edges, and thus it is not adapted for trace element and impurity detection. Several variants using other contrast types were also developed. We will mention here first the use of X-ray reflectivity contrast [11–13]: sub nm height topographic contrast is reached. X-rays reflected from different steps (terraces) on the sample will interfere differently, resulting into changes of the scattered intensity. Consequently, a contrast change will result into the image, evidencing the height changes (atomic steps) of the sample surface. Another variant is using Bragg scattered signal contrast [14–16] by using X-ray focusing optics (as objective) to create the image of the object, local information about crystalline defects in the sample can also be accessed.

Scanning X-ray microscopy exploits highly focused X-ray beams to obtain information in each pixel while laterally scanning the sample, for answering the key material characterization questions concerning the elemental composition, local chemistry, crystal structure, and material defects. The coherence of the X-ray beam also has key importance and will be discussed later on in the paper. Sub-μm spatial resolution is obtained at highly brilliant synchrotrons by de-magnifying the X-ray source. Modern developments drive towards smaller and smaller focused X-ray beams [17] and as such, state of the art hard X-ray microscopes are approaching towards standard user operation at sub-100 nm resolutions. Several X-ray focusing optics are available nowadays, each of them having their advantages and inconveniences [18]. Focused X-ray spots of sub-10 nm in the hard X-ray regime start to be available for experiments, but one has to have in mind other factors when designing a micro/nanobeam X-ray experiment: chromaticity, beam stability and photon flux, easiness and flexibility of the setup, beam coherence, etc. [18]. This improving spatial resolution achievable by X-rays is narrowing the spatial resolution gap with electron microscopy methods. Hard X-rays also allow for studies in 3D, though the investigation of 3D nanostructures, their chemistry and crystalline structure is still very challenging. The higher beam transmission of hard X-ray photons through the sample is one of their advantages compared to soft X-rays, which makes tomographic approaches on high density materials and/or thicker samples possible. Moreover, recently achievable high intensity X-ray nano-beams are approaching the limit of radiation damage

even for hard condensed matters [19–21].

Scanning hard X-ray spectro-microscopic imaging opens unprecedented complementary possibilities in the study of inhomogeneous samples at the micro- and nano-meter scale with high analytical sensitivity. It gives insight into the spatial variation of the major and minor sample components, impurities and dopants by X-ray Fluorescence (XRF) and their chemical and electronic states by X-ray absorption spectroscopy (XAS). XAS can be measured either by detecting the emitted XRF signal in case of trace elements or by transmission signal detection in case of major components. However, the use of X-ray spectro-microscopy as primary technique is still not widespread in materials sciences in spite of the fast development during the last twenty years [7,22–25] and their combination with other complementary techniques [23,26,27]. Recent advances permit the detection of impurity clusters of down to ~20 nm dimensions [28–30]. The combination of X-ray nano-computed tomography and nano-XRF has been demonstrated for the structural and chemical study of nanoscale inhomogeneities [31]. The improvement of detection speed and advanced detectors permit fast scanning to map metal impurity distribution and to get insight into their chemical state. This opens emerging hierarchical characterization [30,22] to study challenging tasks demanding large field of views with small spatial resolutions, such as metal nano-defect clusters (typically tens of nanometers size) embedded in the sample matrices and the characterization of the chemical states of metals and local atomic disorders including atomic configuration, elucidating the chemical origins and stability of such clusters, impurities and dopants [32,33].

The combination of different X-ray analytical techniques complementary to scanning spectro-microscopy, such as μ-/nano- X-ray diffraction, scanning absorption-, phase- and dark field imaging, X-ray coherent scatter imaging, or X-ray excited optical luminescence (XEOL), provides access for probing the variation of strain, stress, crystalline structure, electron density, sample granularity, and to optical characteristics respectively. By the combination of the extremely high-lateral resolution of scanning probe microscopes, providing key information on surface morphology and local physical properties with a resolution going down to the atomic scale, and of X-ray techniques, even nm-scale elemental and chemical mapping is becoming possible [34,35].

Scanning hard X-ray microscopic imaging using X-ray diffraction (XRD) contrast is another emerging technique. Similarly to the spectroscopic ones mentioned above, the approach uses the signal diffracted by the regular arrangement of the atoms in a crystalline sample as contrast to generate the sample images. It requires tuning the experiment geometry such to detect and be specific to the chosen XRD signal (i.e. a particular Bragg peak), while laterally scanning the sample in the focused X-ray beam [18,36]. We will point out here that this approach can be compatible, under certain circumstances, with detecting and acquiring simultaneously other signals from the sample (ex. XRF) in a multi-probe and multi-modal approach [7, 37–39]. Once the objects of interest are identified, they are illuminated by the X-ray beam and, without changing anymore the lateral position of the sample, the diffracted signal is characterized into details (e.g. by mapping it in the reciprocal (Fourier transform) space). Modelling the data allows extracting information about the crystalline phases, composition and/or strain. Rather new techniques made use of the coherence of the X-rays available at synchrotron sources. Approaches like X-ray holography, Coherent Diffraction Imaging (CDI) or Ptychography emerged and allow pushing the lateral resolution for sample characterization (electron density and strain) to the sub10 nm limit. They will be detailed later on in this paper.

These technological and methodological developments enable new experiments that have not been possible before; experiments requiring high-lateral resolution, large fields-of-view or statistically meaningful data, and three- (or even multi-) dimensional multi-technique analysis. The construction of new material science oriented hard X-ray nanoprobe beamlines and set-ups show the importance of these techniques [18,22,40]. If combined, the emerging suite of electron and x-ray structural probes will enable characterization over all hierarchical length scales ranging from atomic to mesoscopic scales [19,23,41].

In this paper, we aimed to illustrate the present status of X-ray based microscopy techniques at synchrotron sources (in the field of materials science) via some selected examples and bibliography. We are aware that they are neither exhaustive nor complete; the choice of the cited papers is necessarily biased by our partiality and personal choice; we apologize to the authors feeling this choice is partial and unfair for them

2. Materials and Method

2.1. Scanning X-ray Fluorescence Microscopy

X-rays having energy larger than the binding energy of an internal shell of an element can knock out an electron from the inner core. The resulting ion with a core level vacancy is in a high energy unstable configuration, and will restore equilibrium by an electron transfer from a higher energy outer electron shell. The energy equal to the difference between the two electronic levels will be emitted by the atom either as an X-ray photon or as an Auger electron. The spectroscopy technique dealing with the measurement and interpretation of the X-ray emission lines created during the radiative decay is usually referred to as X-ray Fluorescence (XRF) spectroscopy. The discrete energy values of the X-ray fluorescence lines are related to the atomic number (Z) of the excited atom and are referred to as characteristic lines. This key feature makes XRF spectroscopy a valuable multi-elemental analytical tool for the study of sample composition. The excitation of core shells can be also induced by particles, i.e. proton-induced x-ray emission (PIXE) spectroscopy or electron induced energy dispersive X-rays (EDX). The detailed description of X-ray Fluorescence Spectroscopy can be found elsewhere e.g. [42–44].

The intensity of a characteristic X-ray line is proportional to the intensity of the incoming X-ray beam and to the concentration of the emitting element. XRF spectroscopy provides access to major, minor and trace element information with high (parts per million, ppm) sensitivity. Although absolute quantification might be challenging for certain samples, qualitative or semi-quantitative concentrations can be obtained in a quite straight-forward manner. The challenge of material science applications for XRF is the eventual self-absorption of low Z elements in thick layers and bulk samples. Moreover, the probability of X-ray fluorescence emission, the fluorescence yield, is competing with the probability of the Auger effect, where the filling of an inner-shell vacancy of the excited atom is accompanied by the emission of a higher shell electron (Auger electron) from the same atom. For light elements ($Z < 30$) the Auger effect dominates over the X-ray radiative decay [44], which results in the smaller analytical sensitivity of XRF for light elements.

Information on the 2D compositional variation can be obtained by focusing the incoming X-rays into a μm/nm sized spot e.g. [17,18,22,23,29,30,41] and by raster scanning the sample in the focused beam. The spatial resolution of scanning XRF spectroscopy is determined by the focused

beam-size, by the scanning step-size and by the scanning mode (step by step or continuous). In the case when the focal spot size can be tailored, e.g. by using a secondary source, to match the step-size of the scan, this provides a possibility of zooming [45]. However, if only the step size is varied while the focal spot size remains unchanged in the case of "step by step" scan, the sample will be scanned by jumping from spot to spot, which will result in missing parts of the sample if the beam size is smaller than the step size. Scanning XRF nano-probes are mostly installed at synchrotrons since a high brightness X-ray source is crucial for obtaining an intense nano-beam. The 2D elemental distribution provides only average information over the traversed sample thickness. Information on the internal elemental distribution in three dimensions (3D) can be obtained by X-ray fluorescence tomography [24,37,46–49], where a series of 2D projections of the elemental distribution of the object are acquired at different angular orientations and an adapted mathematical inversion formula is used for the tomographic reconstruction e.g. [50]. This technique can also be combined simultaneously with scattering and transmission tomography providing complete information on the elemental and structural information [37,51]. Scanning X-ray fluorescence tomographic characterization is still relatively rare in material sciences [52], and especially with sub-μm spatial resolution. The implementation of this technique is very challenging on one side due to the high precision necessary in sample positioning, but also due to the eventual radiation damage, which has been observed for condensed matter in some high spatial resolution 2D mapping studies [19–21]. This can be partly overcome by fast continuous scanning of the sample which paves the way towards 3D information within some hours [53–55]. Confocal X-ray imaging e.g. [56] provides information about the 3D internal elemental distribution at some μm's depth resolution; however this method has not yet overcome the sub-μm depth resolution limit.

2.2. Micro- and Nano-X-Ray Absorption Spectroscopy

The fine variation of the absorption coefficient, μ(E), in the vicinity of an absorption edge is the so-called x-ray absorption fine structure (XAFS) phenomenon and the technique of its detection and interpretation is called X-ray absorption spectroscopy (XAS). XAS is a powerful technique, owing to its chemical selectivity and high sensitivity in interatomic distance determination, in the study of the valence state of the investigated atom, its local atomic environment and its electronic structural properties in condensed matters. As such, X-ray absorption spectroscopy has the potential to measure local structural disorder, including atomic configurations, of materials. It does not require long-range ordering of the sample structure, which is an important asset in the study of nano-systems. XAS measures the variation of the absorption coefficient μ(E) of an element by tuning the energy of the probing photon through its absorption edge. The x-ray absorption fine structure is commonly divided, depending on the studied energy range around the absorption edge, into the near-edge region, which is called X-ray Absorption Near Edge Structure (XANES) or Near-Edge X-ray Absorption Fine Structure (NEXAFS), and the extended x-ray absorption fine structure (EXAFS) regions, which are briefly described in the followings. The physical origin of the XAS signal can be explained by means of the scattering theory, in the frame of quantum mechanics. If the energy of the incoming photon is smaller than the E_0 ionization energy of a given core electron shell (pre-edge region), then the core electron can only be expelled to empty bound atomic states. When the energy of the photon is sufficient to eject the electron to the continuum then the free electron can be described as an outgoing spherical wave. If the photoelectron is scattered by the electrons in the surrounding atoms, its wave

function is modified by the atoms' potential and the final state is composed of the outgoing spherical wave and of the backscattered waves that perturb the system. The wave-number of the photoelectron is changing when the photon energy is scanned in the vicinity of the absorption edge; this changing interference causes modulations in the absorption coefficient. This is observed as oscillations in the post-edge region of the XAS spectrum. The scattering effect can be expressed as a sum of contributions due to all possible scattering events. XAS can be measured in X-ray fluorescence yield, X-ray absorption or in total electron yield modes. In the case of diluted and/or thin samples the X-Ray fluorescence yield (FY) is proportional to the absorption coefficient. The FY can be measured by measuring the ratio of the XRF signal and the incoming X-ray intensity around the absorption edge of the investigated element. XAS is widely performed in FY mode in the hard X-ray region, where the fluorescence yield is large (>1%). The fluorescence yield has the advantage of higher signal to noise ratio than the transmission or electron yield detection, and allows measuring XANES for trace elements and diluted samples. However, self-absorption in concentrated and thick samples might be difficult to correct for. As such, FY-XAS is mostly applied for thin and/or diluted samples. In total electron yield (TEY) mode both the photoelectrons and Auger electrons are detected. The TEY is proportional to the absorption coefficient. TEY-XAS can be applied for concentrated and conductive solid samples. It is sensitive to the surface layer corresponding to the average electron sampling depth (~some tens of nm's). In absorption XAS mode, the intensity ratio of the incoming and transmitted beam is measured in the function of the beam energy, using Beer's law to obtain the absorption coefficient. This mode is well adapted to measure minor and major elements and provides average information along the traversed sample thickness. The sample thickness must be considered before measurement, as absorption coefficients vary greatly across the X-ray energy range and among materials. Excellent reviews [32] and books e.g. [57–59] are available for the detailed description of this technique.

The X-ray absorption near edge (XANES) region of the absorption spectrum includes a few tens of eV before and after the edge including the edge jump. XANES spectra probe the partial density of the empty states of the absorbing atoms and are very sensitive to the bond length, to the symmetry of the coordinated atoms, the distribution of charges, and the potential and relative arrangement of multiple atoms. The oxidation state of the absorber can be obtained from the edge position of the XANES. The dependence of XANES spectra on the local symmetry around the central absorbing atom provides access to polarization dependent studies in certain symmetries. Thanks to the scalar product between the photon polarization and position of the electron vectors in the matrix element of the absorption cross section, a linearly polarized X-ray beam makes possible the investigation of the conduction band-states distribution along the different plane of the crystals in case of anisotropic crystal structure. The polarization-dependent XANES measurements can differentiate e.g. between zinc-blende and wurtzite phases allowing structural determination with directional sensitivity.

By using focused X-rays, μ-/nano- XAS provides spatially resolved speciation information in heterogeneous samples or individual nanostructures. For example, information can be obtained around dopant and impurity absorption edges about their incorporation characteristics and oxidation states in the host lattice. XANES or speciation mapping, where several X-ray maps are collected at different energies characteristics to specific XANES spectral features of the investigated absorber, [60–64] can be easily combined with point-XANES measurements. The determination of the oxidation state of transition metals at high spatial resolution is a crucial issue for many fields of science, including condensed matter. Recently Strachan et al. 2011 [65] demonstrated nano-XANES

and XANES mapping in near *in operando* condition at sub-100 nm spatial resolution. XANES tomography providing information about the internal valence state distribution can also be obtained [66].

The EXAFS region of the X-ray absorption spectrum starts at a few tens of eV after the edge and can be extended up to more than 1 keV. The EXAFS signal results in a series of oscillations with respect to the edge jump. EXAFS mainly probes the radial arrangement of the neighboring atoms around the absorbing atom. The EXAFS technique is very challenging at micrometer and nanometer spatial resolutions, especially in the study of single and heterogenous nano-structures [32,33,67] due to the crucial stability requirements of the beam position and size together with the energy calibration stability of the monochromator. The XANES and the EXAFS regions provide complementary information on the electronic and geometric structure of the excited atom.

Spatially resolved information on the oxidation state can also be obtained by using full-field transmission X-ray microscopy at different energies around the absorption edge of major elements. This approach ensures larger field of views and faster acquisition times which can be advantageous for time resolved, kinetic or *in operando* studies [1,10,25,68]. However this technique cannot be used for the study of trace elements, where scanning probe with X-ray fluorescence is needed for the detection of the XRF signals emitted isotopically into 4π steradian.

2.3. Micro- and Nano- X-Ray Excited Optical Luminescence (XEOL)

When excited by a x-ray beam, luminescent samples may emit visible radiation. This phenomenon is known as x-ray excited optical luminescence (XEOL). The XEOL signal arises after the absorption of an X-ray photon, when the relaxation by the emission of an X-ray photon leaves a vacancy at a higher energy shell. This vacancy will be again filled by a higher energy electron and as such the relaxation proceeds in a cascading manner. When the outermost electrons from the excited atom also become involved, a visible luminescence may be generated in the parent material. XEOL has the advantage of providing information on the light-emitting sites adding site selectivity to XAS. The simultaneous combination of high resolution XEOL and XRF imaging can provide new insight into the role played by impurities in optical luminescence and on the chemical origin of luminescent states from complex nano-hetero-structures and recombination path-ways e.g. [23,69], which cannot be obtained directly by any other technique. The radiation from synchrotron sources is pulsed in nature enabling detection of time-resolved x-ray excited optical luminescence (TR-XEOL) [69,70].

The collection of photoluminescence yield (PLY) by scanning the energy of the excitation x-ray beam across the edge of a luminescent element present in the sample, results in the optically detected XAS (OD-XAS). The first OD-EXAFS spectrum was reported at the Ca K-edge of CaF_2 by Bianconi et al. [71]. OD-XAS probes only the sites of the investigated atoms, which are involved in luminescence emission; as such it provides complementary site-selective information to above described XAS detection modes. The characteristics of the OD-XAS of the specific local sites are determined by the attenuation lengths of the X–ray and optical photons, the inter-atomic excitations, and the sample composition [e.g. 72,73]. XEOL and OD-XAS are well suited for the study of light emitting thin films and devices [74].

2.4. Micro- and Nano- X-Ray Diffraction (XRD) Microscopy

X-ray diffraction (XRD) signal can also be used as a contrast to generate the raster maps, combined with the use of a focused hard X-ray beam. The position of the sample will have to be laterally scanned; we can think of either having an inhomogeneous crystalline object (different crystalline phases, mixture of crystalline and amorphous) or a well crystallized and epitaxial one. In the first case, placing an area detector with an angular opening large enough to intercept enough of the XRD rings (wide 2θ range to allow phase identification) and using transmission geometry in scanning mode is the most appropriate and easy to implement. The angular stability of the sample is not (or less) of a concern, and most of the time the position of the detector is fixed. In the second case, the constraints of the experimental setup are increased. While scanning the sample laterally, a specific point or region of the reciprocal space is to be accessed. Thus, the scanner stage will need to include rotations and be mounted on an adapted diffractometer; the parasitic angular movements (wobble) have to be minimized, and the sample has to remain in the X-ray spot when the sample is angularly rotated [18].

A technique similar to Scanning XRF Microscopy is used for obtaining XRD microscopy. The sample and detector are placed in (angular) conditions to measure the scattered intensity (Bragg peak) of a characteristic signal of the object: this can be related to its lattice parameter (different of the substrate), shape of the object or strain inside it (e.g. by a broadening or displacement of the Bragg peak). Without changing the detector and sample angles set up to be sensitive to the chosen signal, and laterally scanning the sample, a diffraction contrast map is obtained [36,75]. Then, a particular sample area or nano-object is chosen and characterized into detail using XRD approach: the sample is laterally positioned in the X-ray beam, then, without moving anymore the sample laterally, the angle positions are scanned in order to measure the distribution of the X-ray scattered intensity in the reciprocal space (reciprocal space maps, RSM). By simulating this signal, the characteristics of the object can be retrieved: mainly strain value and its distribution inside the object, but also some information about shape, size, etc. By using X-ray beam of small lateral dimensions, sub-features of the objects can be illuminated and characterized by XRD [15,75–79].

2.5. Making use of the coherence of the X-ray beam

We have shown before that the use of intense and small size X-ray beams is a pre-requisite of performing hard X-ray microscopy experiments. If we consider as well the need of possibility to tune or scan the energy of the beam to access vicinity of absorption edges, the choice of using synchrotron radiation becomes rather obvious. What we described up to now is not making use of an important property of the X-rays generated at synchrotrons, i.e. their enhanced coherence (compared to “classical” sources available at most research laboratories). Indeed, in a “classical” diffraction experiment, the phase of the scattered beam is lost and only its amplitude (intensity) is recorded. Several novel approaches developed lately are using the coherence of the X-rays and gain access to the phase information, information which is somehow encoded into the recorded data. We will try in the following to briefly remind them and give a few examples. The reader interested into more details about the experimental setup (coherent focused X-ray beams), the measurement and anlaysis techniques, and the corresponding theoretical description can find more information in [18] and references therein.

2.5.1. Holographic like approaches

In holographic like approaches we can talk about a "direct encoding" of the phase information in the recorded data. The photons which are scattered after the interaction with the sample will interfere with an undisturbed wave, resulting in an interference pattern recorded by the (area) detector. The reconstruction can be done either by illuminating the recorded data by another reference wave or numerically via computer based routines. Several variants (using focused X-ray beams) are available [18]. We will briefly mention here:

i) in-line (Gabor) holography is realized for samples for which a significant (several 10%) part of the beam is transmitted through (unmodified by) the sample structure. This part of the beam will constitute the reference (undisturbed) wave which will interfere with the wave distorted following its interaction with the sample, to create the hologram. The interference pattern (hologram) is recorded by the area detector, and can be "reconstructed" (as mentionned above) either by illuminating it by the reference plane wave (generates the real and virtual images of the object) [80] or numerical approaches ex. [81]. We will note here that the "real" and "virtual" reconstructed images superimposes on the same beam path (twin image problem).

ii) off-axis holography [82]: the major change with respect to the in-line holography is that the reference wave is no more collinear with the object detection axis but it has an offset angle. One approach to do this is detailed in [83]: Kirkpatrick-Baez (KB) mirrors illuminate a pair of waveguides; one is used to illuminate the sample, while the other to supply the reference wave. The "real" and "virtual" reconstructed images are angularly separated from each other.

iii) Fourier transform holography: one or several reference objects (R), placed in the vicinity of the object (O) to be measured, are used to generate the reference wave which will interfere with the wave scattered by O. Since the first measurements in transmission mode [84,85], it was also proved in Bragg reflection geometry with focused X-ray beams (see for ex. [86]). In addition to the 3D shape of the object (electron density), access to internal displacement field is also possible. We will point out here the rather important constraint of the presence of reference object(s). Moreover, in the case of Bragg geometry, the reference object has to be not only very small (its size is basically given by the spatial resolution) but crystalline as well [77].

2.5.2. Coherent Diffraction Imaging

This approach is based on computer algorithms and methods for phase retrieval from Coherent Diffraction Imaging (CDI) data. There are at present number of methods, algorithms and principles, proofed and used for the phase retrieval, the interested reader can see the bibliographic work done in [18] (Chapter 7), [87].The first experiments [88] were used to obtain the morphology of a flat sample containing (nano-)objects placed in the illuminated X-ray spot, i.e. the projected electron density along the X-ray beam direction. 3D tomographic approach (recording 2D measures at different azimuth angles, and volume reconstruction) followed rapidly [89]. Using of focused X-ray beams to reconstruct objects in 3D was also demonstrated [90]; the use of increased photon fluxes allowed reducing the size of the investigated objects and increasing the lateral resolutions in the reconstructed data.

The following step was in fact to retrieve not only the shape, but also to access (to image) the strain inside these objects, and, if possible, with the same good lateral resolutions as the one for the

shape reconstruction mentioned above. If the first demonstrations were proposed using a planar (not focused) X-ray beam, which makes simpler the concept of the data treatment, the use of focused beams and curved wave fronts was also later considered [91–93]. Indeed, like mentioned before, the gain in photon flux density (thus smaller object sizes and better spatial resolution accessible) can easily counterbalance or overcome the more complex theoretical description and reconstruction algorithms. For example, different situations were identified in the review [18], each of them having its own subtleties (specific algorithms):

i) weakly non-homogeneously strained crystals [94–97].

ii) highly non-homogeneously strained crystals [98–100].

iii) Fresnel CDI [100,101] was proposed in order to avoid so called "trivial solutions" in a support based phase retrieval imaging approach (phase offsets, conjugation errors, variations in position of the reconstructed object). If Fresnel diffraction is used, combined with an incident wave having a known, non-zero and finite curvature, then a unique solution exists. The curved wave field can be produced by focusing optics, and the object of interest is not anymore placed at the focal point, but, on purpose, out of the focal plane (i.e. the illuminating wave front is significantly curved). The detector is placed in the far field regime. The numerical reconstruction involves firstly the accurate reconstruction of the complex valued illumination wave front [93,101,102], then the phase retrieval is performed on the scattered data.

2.5.3. Ptychographic methods

The method makes use of specifically created redundancy in data measurement algorithms: the sample is illuminated by a (coherent) finite-size X-ray spot and the interference scattered pattern is recorded. Then a similar measurement is recorded by laterally shifting the sample, but on a lateral distance significantly smaller than the size of the focused X-ray spot (illuminated area). There is thus a significant oversampling concerning the illuminated area. The sample scattering function can then be reconstructed. The illumination function does not have to be a plane wave anymore; moreover, due to the data redundancy, the reconstruction algorithm will also reconstruct the exact illumination function (no pre-knowledge necessary). Several algorithms were proposed [103–106]. If the first step was consisting of planar views reconstruction, tomographic reconstructions were also performed [107]; Bragg variant was also demonstrated [108,109].

2.6. Other Complementary X-Ray Microprobe Techniques

2.6.1. Scanning Transmission X-Ray Microscopy (STXM)

Possibly one of the easiest approach in raster imaging mode with a focused X-ray beam, is to record the transmitted signal for a thin specimen by Scanning Transmission X-ray Microscopy (STXM) [18,110]. The corresponding map is related to the variation of the absorption contrast due to electron density inhomogeneity or sample thickness variation. In case of uniform sample thickness, the resulting map is related to the projection of the material density along the X-ray beam direction. The lateral resolution of STXM is essentially given by the lateral size of the X-ray beam. A variant of this technique makes use of an area (2D) detector. Apart the intensity of the transmitted beam, its positon (center of mass) on the area detector can be calculated and its deflection (due to refraction

effects) measured, with respect to the initial position (no sample). These deflection values (ex. in x and y directions) can be used as contrast mechanisms to trace the raster map of the sample (differential phase contrast image measurement [54] and references therein). In a similar way, the Small Angle X-ray Scattering (SAXS) signal can be detected and used to generate the contrast in the raster maps [38,111].

2.6.2. Full field microscopy techniques

We already mentioned that various contrasts can possibly be used in full field microscopy techniques: i) Absorption; ii) Phase contrast [112,113] with the variant of Grating based imaging/X-ray Talbot interferometry [114–116]; iii) X-ray reflectivity [11–13]; iv) Bragg scattered signal [14–16]; v) fluorescence [117]. An area detector is used in all these cases to generate a 2D (projection) image of the sample but 3D approaches can also be foreseen. Without entering too much into details, one of the most important advantages of the full field techniques is obtaining a full (2D) image in a single acquisition, even if the exposure time can be or is much larger than the dwell time per pixel in the raster map (generally true for XRF mapping). The total data acquisition time is still generally lower compared to the total time when performing the raster mapping approach [14].

3. Results

State of the art X-ray spectro-microscopy techniques provide unprecedented elemental and chemical specificity with the possibility of obtaining complementary information on the structure, morphology, and crystalline structure by other complementary X-ray techniques (see Figure 1). This opens new opportunities for the study and engineering of new materials and new technologies, for creating e.g. electrochemical, thermoelectric, photovoltaic devices, nuclear materials [118], nano-wires, nano-devices for memory, sensing, logic, light emission and wave-guides. The triggered technological developments make available lower production costs, higher efficiency, more flexibility, simplified designs and improved safety.

A large amount of work has been devoted to the characterization of semiconductor samples including multicomponent alloys, nano-systems and nano-structures. Precipitates, their size and density variation, chemical state, and eventual multiphase precipitations highly influence and alter the characteristics of these samples. Material defect interactions, the association of impurities with structural defects and doping induced changes govern the performance of many emerging technologies. However the small size and the low density of metal precipitates render the application of standard analytical tools difficult, where the high sensitivity and high spatial resolution achievable by modern hard X-ray microscopes provides a real asset. Clearly, the study of such materials and devices at hierarchical length-scales [30] also in *in situ* and *in operando* [25, 119–121] is becoming crucial both for improving fabrication processes and to answer challenging questions from a fundamental point of view.

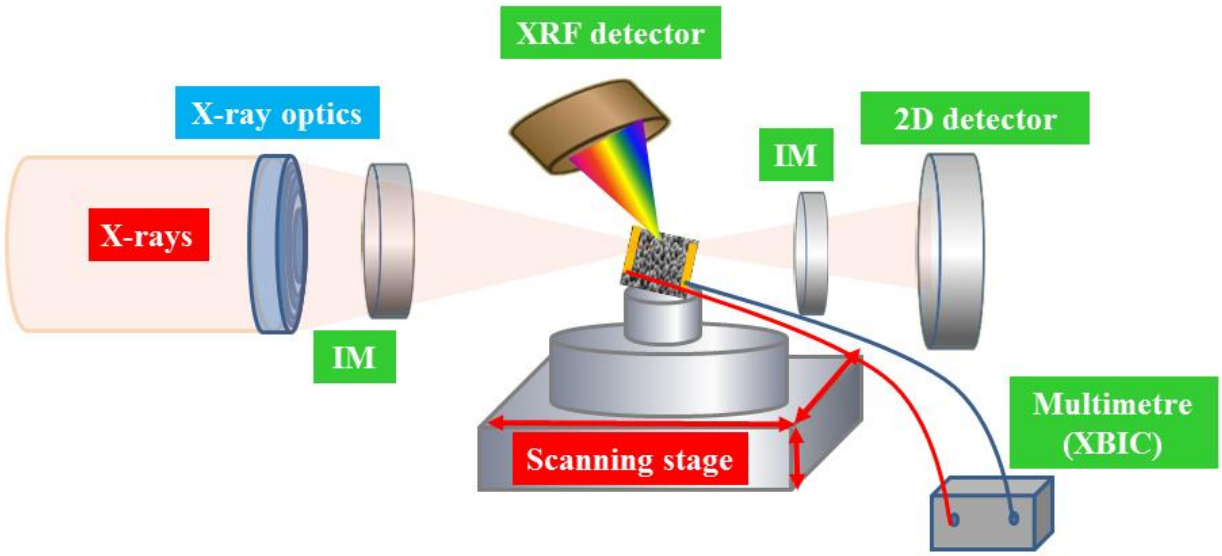

Figure 1. A possible scheme of a multi-technique scanning hard X-ray microscope showing the focusing optics creating the highly focused nano-beam at the sample position; the XRF detector collects the characteristics X-ray spectra, the IM intensity monitors (e.g. photodiode) are used for intensity normalization, for XANES /EXAFS in absorption mode and for absorption contrast measurements, the 2D detector is used for X-ray transmission contrast measurements, such as absorption-, differential phase- and scattering contrast, while other contrasts such as X-ray beam induced current (XBIC) studies are also possible to implement.

The fabrication of nanometric-sized self-assembled structures is an important way of enhancing the device performance. For example nanowire (NW)-shaped semiconductor photovoltaic and light emitting devices have been shown to absorb light in a much more efficient manner allowing to further improve their characteristics. Even flexible devices can be constructed by NW morphology. Bulk methods can only measure average out characteristics overlooking small-scale effects and local differences within the samples. Only techniques offering micro- or nanometer scale spatial resolution and high sensitivity can be applied for individual nano-object characterization.

X-ray spectro-microscopy is mostly applied to track structural and chemical changes at the nanoscale as a complementary tool to the analytical techniques frequently used for the characterization of these nano-objects, such as transmission electron microscopy (TEM), and scanning electron microscopy (SEM) also coupled with energy dispersive spectroscopy (EDS), electron energy-loss spectroscopy (EELS), secondary ion mass spectrometry (SIMS) and nano-SIMS, cathodoluminescence microscopy and spectroscopy, three-dimensional (3D) composition evolution by advanced TEM, correlated atom probe tomography, focused ion-beam (FIB) tomography. The aforementioned non-destructive in-situ and in operando capabilities and high trace sensitivity of X-ray spectro-microscopy is a significant asset to obtain complementary information compared to these laboratory techniques.

3.1. Study of heterogeneous materials/samples

3.1.1. Si-based Solar Photovoltaic

Only a niche market a few years ago, solar photovoltaic is now becoming a mainstream electricity provider. Solar photovoltaic was one of the first technologically interesting materials studied by synchrotron based spectro-microscopy techniques, where μ-XRF and μ-XAS investigations played a major analytical role in the fast development [28–30,61,122–130] (see Figure 2). Based on the needs of these investigations, important fields of microscopic research emerged: the detailed characterization and improvement of doping microstructures and microdefects, which significantly limit the device performance.

Multi-crystalline (mc-)Si materials show, as a rule, significant spatial variations of defect densities and related material characteristics. The first μ-XRF investigations e.g. [122] of multi-crystalline-silicon solar cells provided the first direct evidence that transition metal agglomerates play a significant role in their performance, forming regions of high minority carrier recombination centers. Simultaneous μ-XRF and x-ray-beam-induced current (μ-XBIC) measurements [123,124] enabled the in situ study of the relation of the chemical nature of the defects and impurities, and their recombination activity. The work of Buonassisi et al. [28] combining μ-XRF, μ-XAS and μ-XBIC, showed that the size, spatial distribution and chemical binding of metals within clusters is just as important as the total metal concentration in limiting the performance of multi-crystalline silicon solar cells (see Figure 2, panel a). Even large amounts of metals turned out to be acceptable as long as their size and spatial distributions are properly engineered. Metal nano-defect clusters embedded in a semiconductor matrix have small size (typically tens of nanometres) and comparably large separating distances (up to tens of micrometers). The arrival of high spatial resolution hard X-ray nano-probes allowed for the detection of transition metal precipitates of the order of some ten nanometers dimensions [29,30,125]. These measurements showed the crucial need for hierarchical multi-scale characterization for statistically significant studies [30].

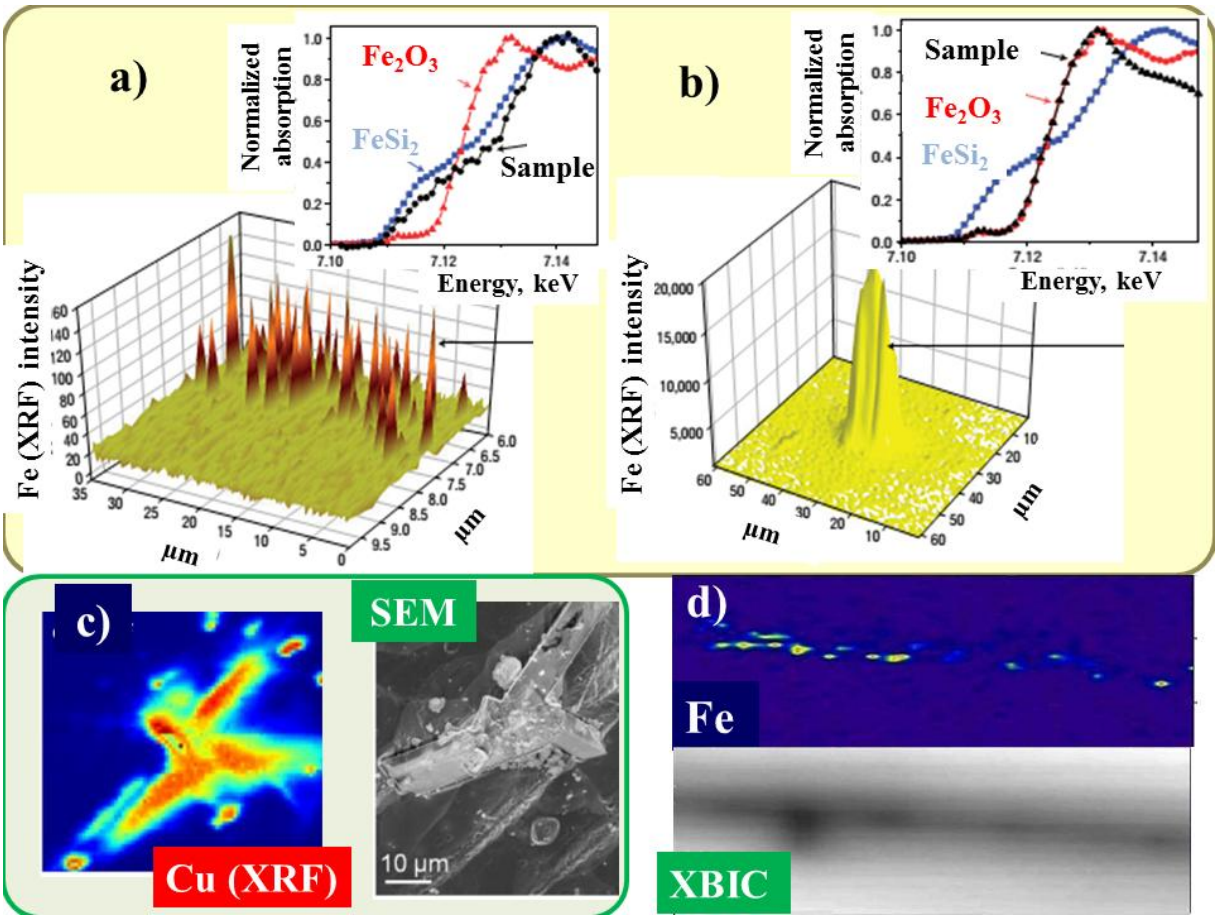

Figure 2. Analytical possibilities of scanning X-Ray Spectro-microscopy and complementary techniques for the study of transition metal (Fe, Cu) precipitates in mc-Si solar cell materials. a) and b) scanning XRF and nano-XANES provides information about the different types of metal defects in commercial solar-cell material. a) the distribution of iron nano-precipitates with 20–30 nm size was revealed by scanning XRF, while the nano-XANES measured within these preticipitates (sample: black XANES curve) are iron-silicide (blue XANES curve: $FeSi_2$ standard). b) Fe inclusions with several µm's in diameter are composed of iron oxide (red XANES curve: Fe_2O_3 standard) (from ref. [28] Buonassisi et al., reprinted with permission N° 3592150804171 from Macmillan Publishers Ltd: Nature Materials) c) the high analytical sensitivity of scanning µ-XRF can be combined with the high spatial resolution of electron microscopy techniques, here Scanning electron microscopy (SEM) reveals a N_4Si_3 micro-crystal co-localized with Cu containing defect, high Cu intensity is in redcolors (from ref. [131] Zuschlag et al. with permission of Trans Tech Publications N° 3596760493275) d) X-ray induced current (XBIC) measurements are frequently used in combination with spectro-microscopy for studying the correlation of precipitate chemistry and electrical activity. Here Fe micro-precipitates detected at grain boundaries shows inhomogeneous electrical activity as identified by µ-XBIC. (from ref. [127] Trushin et al., with permission N°: 3592141336062 from Elsevier).

These findings triggered a strong need to understand the physical and chemical properties of metal clusters and metal-structural defects interactions [126] and their effect on the local device characteristics and behavior in solar cells [29,61,127]. Electrical properties of intentionally contaminated mc-Si materials were investigated in relation with the distribution and speciation of transition metals, to gain insight into the relation between size and chemical state and the likely origin of clusters [127] (see Figure 2, panel c). The understanding of the underlying mechanisms of the recombination activity of transition metal precipitates is a matter of fundamental scientific interest with direct impact on industrial applications. Experimental evidence is crucial to validate the theories of the possible recombination mechanisms. Quantitative stress mapping and recombination activity measurements by simultaneous micro-photoluminescence spectroscopy (μ-PLS) and micro-Raman spectroscopy (μ-RS) and complementary nano-XRF were performed by [128] for investigating the correlation between the size of the transition metal precipitates, the induced stress and the recombination activity. Theoretical models closely predicting the performance of experimental cells were developed [128-130] permitting simulation-guided process optimization and defect engineering, in order to improve the quality of even heavily contaminated mc-Si materials. This paved the way towards efficiency and yield enhancements and an entirely new approach for fabricating cost-effective solar cells from abundant but impurity-rich feedstocks.

3.1.2. Nitride Semiconductor Materials

Scanning spectro-microscopy and its combination with other complementary techniques provided important information also on nitride semiconductor materials. Gallium nitride is a widely used semiconductor material, which has wide field of application e.g. as light emitting (LEDs) and laser diodes, wide band gap energy applications, micro-wave radio-frequency power amplifiers, solar cells, as well as being the key material for next generation high frequency, high power transistors capable of operating at high temperatures. The application of electronic and optoelectronic devices based on nitride semiconductors is growing extremely fast, but the fundamental science underlying these devices is lagging behind. As such, exploring the vital link between structure and properties is crucial and profit from new complementary characterization possibilities. The key strategy is to combine multiple microscopy techniques to develop a comprehensive understanding of defects in nitrides. This requires assessing the same nanoscale regions of material in multiple microscopes, so that the structure and composition of a specific nanostructure may be linked directly and unambiguously to its electrical and optical properties. Overall, the aim is to provide a much more complete picture of nitride materials than has ever previously been achieved, and to apply this new understanding to engineering improved materials for working devices. For example the tailoring of the characteristics of nitride based semiconductors, as the band gap size and the related color of light emitting diodes, or the magnetic characteristics by creating diluted magnetic semiconductors [132], can be achieved by different doping. One of the key questions of doping is whether the resulting material is indeed an alloy or whether it remains as GaN with clusters, precipitates or second phases, which are determining the new properties.

As an example, the ideal diluted magnetic semiconductor (DMS) is a semiconductor material doped with a ferromagnetic (FM) impurity, presenting ferromagnetism above room temperature. Despite the many investigations, the origin and control of ferromagnetism in DMSs introduced e.g. by Mn or Co doping is one of the most controversial research topics in materials science and

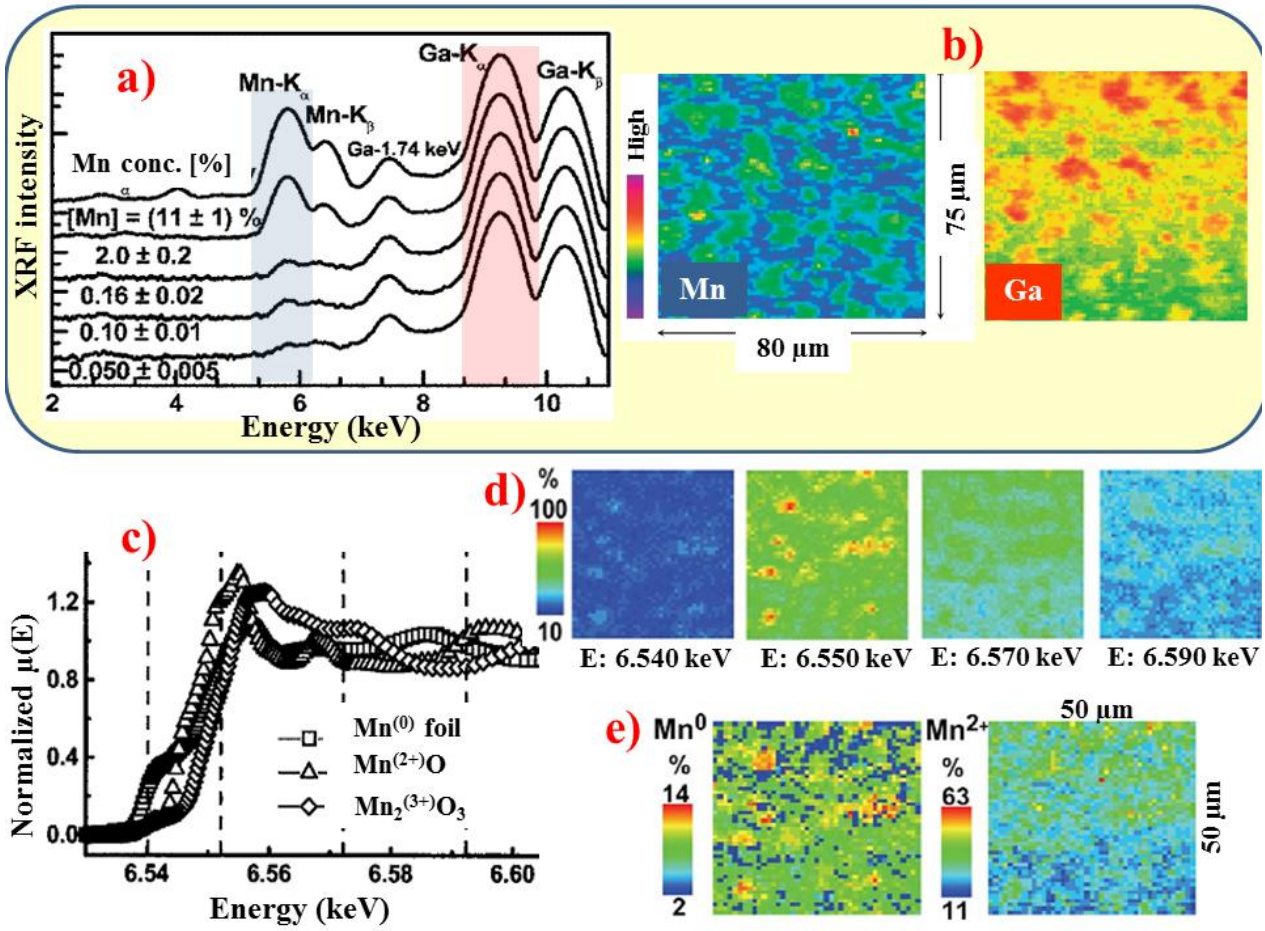

Figure 3. Scanning X-ray spectro-microscopy study of Mn-doped GaN. a) XRF average spectra of GaN samples containing different Mn dopant concentrations. The Mn concentrations determined by XRF are indicated in the figure. The Mn-Kα (blue) and Ga-Kα (red) XRF peaks were chosen for obtaining the spatial distribution maps. b) Ga and Mn distribution in the highly Mn-doped GaN sample containing 11% Mn. (Copyright 2004 The Japan Society of Applied Physics from ref. [133] Martinez-Criado et al. 2005) c) Normalized x-ray absorption spectra near the MnK-edge for several model compounds with known valencies from zero (Mn metal foil) to three (Mn_2O_3). The characteristics energies used for XANES mapping are marked by dotted lines. d) Mn intensity distribution maps measured at characteristics energies around the Mn K-edge (see panel c). e) Reconstructed spatial distribution of Mn^0 and Mn^{2+} in the highly doped GaN:Mn sample (reprinted with permission N°: 3592161399803 AIP Publishing LLC from ref. [60] Martinez-Criado et al.).

condensed-matter physics today. The first X-ray spectro-microscopy studies combined with Raman and photoluminescence measurements [133,134] studied the cluster formation induced by Mn-doping in GaN with µm spatial resolution (see Figure 3 panel a and b). Defects induced during Mn-doping were showed to lower the GaN lattice symmetry. Mn incorporation substitutional to Ga was supposed creating a tensile strain in the GaN layers. The substitutional Mn incorporation to Ga

was confirmed by X-ray spectro-microscopy [135,136] for all Mn concentrations studied. These studies suggest continuous change of the Mn valence with increasing Mn content, being close to 2+ in ferromagnetic samples. The spatial variation of the valance state of Mn in the function of Mn doping concentration could be mapped by [60] (see Figure 3, panel e) with an approach of collecting two-dimensional 2D x-ray fluorescence maps at preferential monochromatic energies, which excite different Mn oxidation states. The pre-edge structure of XANES compared to ab initio calculations [135,136] provided indication about the possible band structure of $Ga_{1-x}Mn_xN$ alloys. Polarization-dependent XANES measurements [133,135] capable of discriminating between the cubic zincblende and hexagonal wurtzite GaN polytypes or their eventual co-existence as mixed phase, identified wurtzite structure within Mn clusters independently of the Mn dopant content.

3.2. Investigation of individual nanostructures

Starting from the demonstration of the first QW laser (in the 1970's), low-dimensional materials attracted increasing interest from both fundamental and technological points of view. Semiconductor materials are evolving toward the development of more complex low-dimensional systems and hetero-structures with nanometric sizes. The low dimensionality of these structures and devices gives rise to quantum confinement phenomena, which modify their structural, optical, chemical and electronic properties obtaining unexpected characteristics and improved functionalities. Low-dimensional systems are generally labelled as nanostructures as quantum confinement usually occurs at the nano-meter scale.

Nanostructures and the related functional nanoscale devices have gained great interested in the last decades in several fields such as heterogeneous catalysis, solar cells, sensors, electrical devices, batteries, light emitting diodes, lasers, optoelectronic and spintronic nanodevices, integrated semiconductor spintronics, and quantum information technologies. The development of such applications requires a deep understanding of the physical properties of the nanostructures. On the other hand, the study of ensembles averaging among thousands of nano-structures with slightly different peculiarities can hide important characteristics. For example in oriented systems, such as nanowires (NWs, 1D systems exhibiting nanometric size in two dimensions), the bulk measurements can lead to erroneous conclusions, as was demonstrated by Farvid et al. [137] in the case of the Mn magnetization measurements of Mn:GaN NWs. Here the net magnetic moment determined from single NW measurements was nearly two orders of magnitude larger than the saturation magnetic moment obtained by the ensemble measurements. This is due to the random orientation of the NW's on the growth substrate; since the Mn magnetization of a single NW strongly depends on its orientation with respect to the external magnetic field, the moments for opposite NW orientations will cancel out in the case of ensemble measurements. Any significant magnetization measured for randomly grown NW samples would, therefore, likely to be of extrinsic origin.

Therefore, the study of single nanostructures is crucial. Nevertheless systematic structural and chemical study is also needed at multi-length scales in order to link the characteristics of the basic individual building blocks to that of nano-devices. In spite of this strong need, only few experimental techniques have the required sensitivity, specificity, and spatial resolution to directly probe the structural and chemical state of the dopants, impurities and the electronic structure in single nanostructures. When the excitation matches the energy of an electronic transition, resonant Raman scattering (RRS) can be used to study single NWs. In XFM the scattering background is many orders

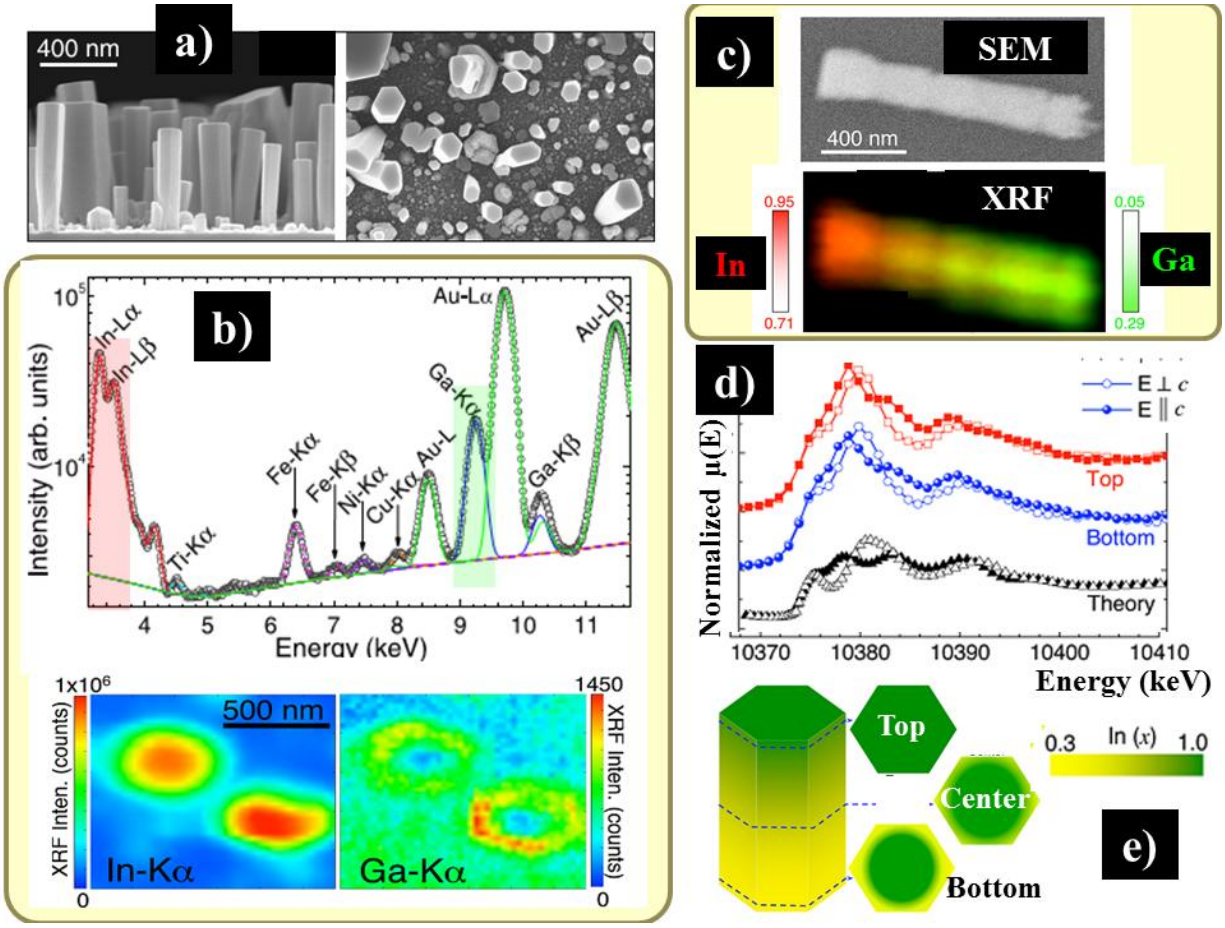

Figure 4. a) SEM images of as-grown $In_xGa_{1-x}N$ nanowires (NW) b). The In and Ga characteristic X-ray lines marked on the typical average XRF spectrum of an individual NW. The In and Ga distribution of two NW's measured from the top. c) SEM image of a single NW and the In and Ga distribution measured by nano-XRF. d) Polarization dependent XANES around the Ga K-edge proves the conservation of the wurtzite polytype along the NW e). A schematic 3D model of a single NW obtained from the results of combined XRF, XANES and XRD (the latter not shown in the figure) characterizations. Reprinted with permission N°: 3594480065540 from ref. [20] Segura-Ruiz et al. Copyright (2013) AIP Publishing LLC, and from Ref. [138] Segura-Ruiz et al. adapted with permission Copyright (2014) American Chemical Society.

of magnitude lower than the bremsstrahlung background present with electron excitation. As a consequence synchrotron X-ray fluorescence (XRF) nanoprobe provides quantitative composition analysis with excellent relative (ppm/ppb) detection limits while the higher spatial resolution of electron microscopy techniques allows better absolute sensitivity within highly localized structures. e.g. [19,131]. In the case of TEM, SEM the damage caused by the electron beamin the sample [139] is considered to be more important than for X-rays (at least in the case of ≥10 nm X-ray beam sizes and soft matter such as polymers) [e.g. 140]. The use of synchrotron based hard X-ray spectromicroscopy probes is advantageous for the larger information depths, element-, site-, and

orbital selectivity, and chemical trace sensitivity. Electron and X-ray techniques can be combined [23,41] (see Figure 4) for studying with nanometer resolution small embedded domains with weak signals, clusters, dopant segregations, and heterogeneous structures, and for the identification of minority phases, and strain fields.

In semiconductor nanowires (NWs) based on group-III nitrides and their ternary alloys (e.g. $In_xGa_{1-x}N$), compositional inhomogeneities, phase segregation and related strain fields hamper the growth of high quality nano-structures and thus, similarly as in bulk materials, limit the tunability of their characteristics. Up to now, the growth of high crystalline quality without segregation effects still remains a challenge. Several recent works [20,41,138] demonstrated the spontaneous and preferential axial and radial compositional Ga and In inhomogeneity phenomenon in ternary alloy single NW's by nano-XRF with no additional doping and impurity contamination detected. Polarized nano-XANES indicated no secondary phase or metallic cluster formation and the wurtzite structure were preserved within the investigated NWs despite the inhomogeneous elemental distribution (see Figure 4, panel d). Combined simultaneous nano-XRF and nano-XRD [138] allowed to spatially correlate compositional and long-range order information and even made possible to construct a simple 3D model for the analyzed single NW's (see Figure 4 panel e). However, real 3D measurements providing elemental and chemical information at the nano-meter scale [31,141] would be necessary to complement and confirm these suggestions by direct observation, which is still a very challenging task.

NW quantum emitters can enhance several times the optical efficiency compared with standard optical excitation. The enormous demand for superior optoelectronic devices stimulates the application of further optical characterization techniques. Combined synchrotron-based XEOL and simultaneous XRF spectroscopy [142] is a viable characterization tool to study single nanowires with optical and chemical contrast mechanisms with sub-100 nm spatial resolution [143]. This enables the investigation of the underlying mechanisms of optoelectronic nanodevices. Next to spatially resolved XEOL as an imaging tool the time structure of the synchrotron source can also be combined with XEOL [69,70] for performing time-resolved XEOL (TR-XEOL). TR-XEOL provides information on carrier dynamics if the carrier recombination lifetime under investigation is comparable with the time structure of x-ray pulses.

In spite of these recent impressive works in general one of the challenges for future works is performing statistically meaningful number of scans in order link individual and ensemble NW characteristics. This issue started to be addressed in the last years, as shown by the fast acquisition approaches developed recently [54,55,79,144,145]. Such fast and multilength-scale measurements will gain increased importance with the appearance of new diffraction limited storage rings and dedicated X-ray nanoprobes, where several order of magnitude increase in the flux of the nanobeam is expected [146].

3.3. Studies of Individual Micro- and Nano- Objects with μXRD—Selected Examples

XRD methods can give access to the strain inside materials, with a resolution which is hardly achievable by any other technique. Combined with a local probe approach, the local properties (lateral resolution down to nanometer) are accessed. One domain in which this kind of information is of utmost importance, and for which the methods shows its full potential, is related to the studies of semiconductors with potential applications in microelectronics, see for example [2,78,147–149]. On

one hand, the crystalline quality of semiconductors is very good, most of the time they are epitaxial systems. On another, strain is a dominating feature in the resulting properties. Strain engineering in complex systems and via shape, patterning, epitaxy or other manufacturing methods and its accurate characterization are a must, see for example [2,150–152].

The number of examples that the interested reader can find about the contribution of XRD (using focused hard X-ray beams and/or their coherent properties) is extremely large in the literature, including imaging (in 2D or 3D). Number of books and reviews are giving a rather good image about the capabilities of such techniques see for example [21,153–156]. Dedicated facilities, instrumentation (for example dedicated beamlines at Synchrotron facilities) and theoretical approaches are developed and optimized lately.

In the following, we were choosing very particular examples on a particular system (SiGe islands epitaxially grown on Si substrates [2,157] and trying to illustrate not only the contribution of the various XRD like techniques, but their complementarity as well in increasing our knowledge, understanding their properties and optimizing manufacturing and characterization methods towards *in operando* studies. Also selected examples from the literature will be shown. Various shapes close to the square truncated pyramids are most of the time used. The individual objects lateral sizes used in the following examples ranges from about slightly more than 3 μm (Figure 5) down to about 150 nm (Figure 7); the exact shape, size and Ge content highly depend on the growth conditions and sizes in the micron down to sub-100 nm range can be achieved. The epitaxially grown SiGe islands are strained; we will try, via the different experimental XRD local probe approaches, to access quantities which are characteristic of single and particular SiGe objects.

In a first step, a raster map of the sample with XRD contrast will be acquired. The principle is similar to STXM [36]: the hard X-ray beam was focused using Be Compound Refractive Lenses (CRLs) in this particular case and the diffractometer is aligned such that the X-ray spot falls in the center of rotation of all the circles. An optical microscope allows referring this point and pre-positioning the region of interest of the sample at the X-ray beam location [2,18,36,158]. The constraints of the experimental setup are rather important and were pointed out in Section 2.4. The sample and detector are placed in (angular) conditions to measure the scattered intensity (Bragg peak) of a characteristic signal of the object as we are going to see in the following, this can be related to its lattice parameter (different of the substrate), shape of the object or strain inside it (implying a broadening or displacement of the Bragg peak). By setting up the detector and sample angles to be sensitive to this kind of signal, without changing them, and laterally scanning the position of the sample (while recording the detector signal), a diffraction contrast map is obtained.

If the characteristic signal originating from the SiGe islands is detected, a raster map using it as a contrast mechanism will be generated. A particular region of the sample exhibiting a growth defect (and close to the sample edge) was imaged in this case. A superposition of the XRD contrast map and an optical image of the same region of the sample shows it is possible to position and identify single and, most important, particular objects (SiGe islands) in the focused X-ray beam (Figure 5, panel e). Various contrasts maps can be obtained, by appropriately tuning the detector to access the desired position in the reciprocal space. This is illustrated in Figure 5 (panel g) in which the XRD contrast corresponding to the islands facets are used and color coded (see figure legend). We will also point out here that contrast like XRF (Ge fluorescence line in this case) can also be used to obtain the raster maps of this kind of sample, as it was demonstrated in [75].

In the case of more complex samples, this technique ensures the sensitivity to various lattice

spacing (or lattice parameters associated to various crystalline layers), as it was shown for epitaxial tunnel junctions. Each of the constituting layers could have been imaged using lattice parameter contrast (various characteristic Bragg peaks) corresponding to each layer [15,77,159].

Once the objects of interest are identified, they can be individually characterized using XRD methods more into details. The sample is laterally positioned in the X-ray beam, then, without moving anymore the sample laterally, the angle positions are scanned in order to measure the distribution of the X-ray scattered intesity in the reciprocal space (reciprocal space maps, RSM) on individual chosen objects(Figure 5 panels a–d). By simulating this signal, the characteristics of the object can be retrieved: mainly strain value and distribution, but also some information about shape, size, etc. [18,36,160].

We should point out here that in the approach depicted above, some pre-knowledge about the shape of the sample is required. This information is obtained via another microscopy technique, the Scanning Electron Microscopy (SEM). Since the same region of the sample can be imaged, the precise shape of each object is easily identifiable. With this information available, Finite Element Methods (FEM) are applied to model and obtain the strain distribution inside the object. Then X-ray scattered intensity is calculated and compared to the measured one [18,36,160]. The model is adjusted to have a good agreement with the experiment. For this particular sample, these results allowed understanding the growth mode via two steps (flat and truncated pyramidal shaped islands) but also access to the strain distribution inside each of the investigated objects.

With an even smaller beam, it is possible to record XRD signal originating even from sub-structures of the single SiGe objects (for example facets) [75,76] and map their properties into details (Figure 5 (panel g) and Figure 6), like spatially resolving the strain inside the single object. We will see in the next section that this can also be accessed differently, using the coherence property of the X-rays. Using hard X-ray beams of a size which is smaller than the lateral size of the investigated object, local information about precise localization and description of defects inside specific regions of the object (for example, close to their edges) can be performed. Also, it was possible to evidence tilts in the crystalline planes when approaching the edges of the objects; their amplitude and orientations depend on the shape and size of the objects [15,77,161], and were evidenced as well for similar samples by other groups [78] and references therein, [162–165].

If the shape pre-knowledge was required in order to simulate the XRD data recorded for the individual SiGe islands (using SEM for example) new approaches making use of the coherence of the X-ray beam can overcome this issue. As an example, we can mention here the Grazing Incidence Small Angle X-ray Scattering (GISAXS) experiment of [166–168] using an X-ray beam having an important transverse coherent length, on the same type of SiGe islands samples, of various lateral sizes (from 1000 down to 50 nm). By performing GISAXS measurements for different sample azimuths, in a tomography-like experiment, the reciprocal space is reconstructed in 3D close to its origin ($q = 0$) region [166–168]. Then the shape and size of the average SiGe island is modelled and reconstructed. The achieved voxel size in the reconstruction is 10–15 nm and is strongly related to the enhancement of the scattered signal due to the uniformity (shape and size) of the islands.

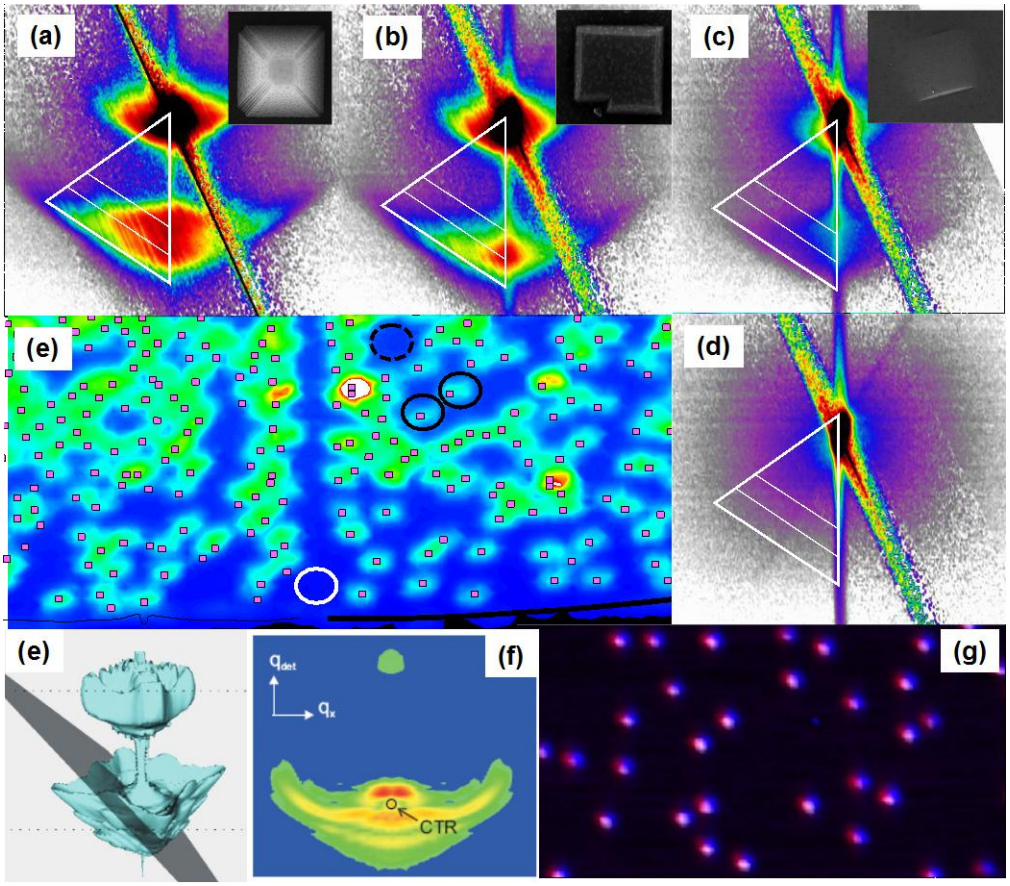

Figure 5. Illustration of method of finding and measuring individual objects (islands) with XRD contrast. Tuning the sample and detector angular values such to measure, in reciprocal space, a position characteristic for the island and scanning the sample laterally, higher intensity is observed whenever an island is illuminated by the X-ray spot, leading to an image of the island distribution (e). Overlaid to it are the island positions (squares) extracted from an optical microscopy image. (a–c) Measurement of the scattered signal close to the (004) Si Bragg peak for individual islands of various shapes (a–c, the corresponding SEM images are shown in the inset). (d) measurement of the scattered signal originating from the empty substrate (vicinity of the (004) Bragg peak). The various intense oblique features in the reciprocal space maps (RSMs) and visible as well in panel (d) (so called detector and analyzer streaks) originate from the particular geometry of the measurement and the use of a 1D detector in this case. (e) 3D RSM image (iso-intensity surface) of the scattered signal (vicinity of the (004) Bragg peak) for a single SiGe island; the presence of the substrate peak (top) and SiGe peak (bottom) can be seen. Note the shape of the signal related to the presence of the 4 side facets on the island. The grey oblique plane represents the region measured by a single area detector image, and is shown in (f). By using an X-ray beam smaller than the size of the SiGe islands, and as contrast signal on the left, middle or right areas in (f) (color-coded by red, white and blue respectively), the generated raster maps (g) are rendered sensitive to the presence of left, top and right side facets of the SiGe pyramids.

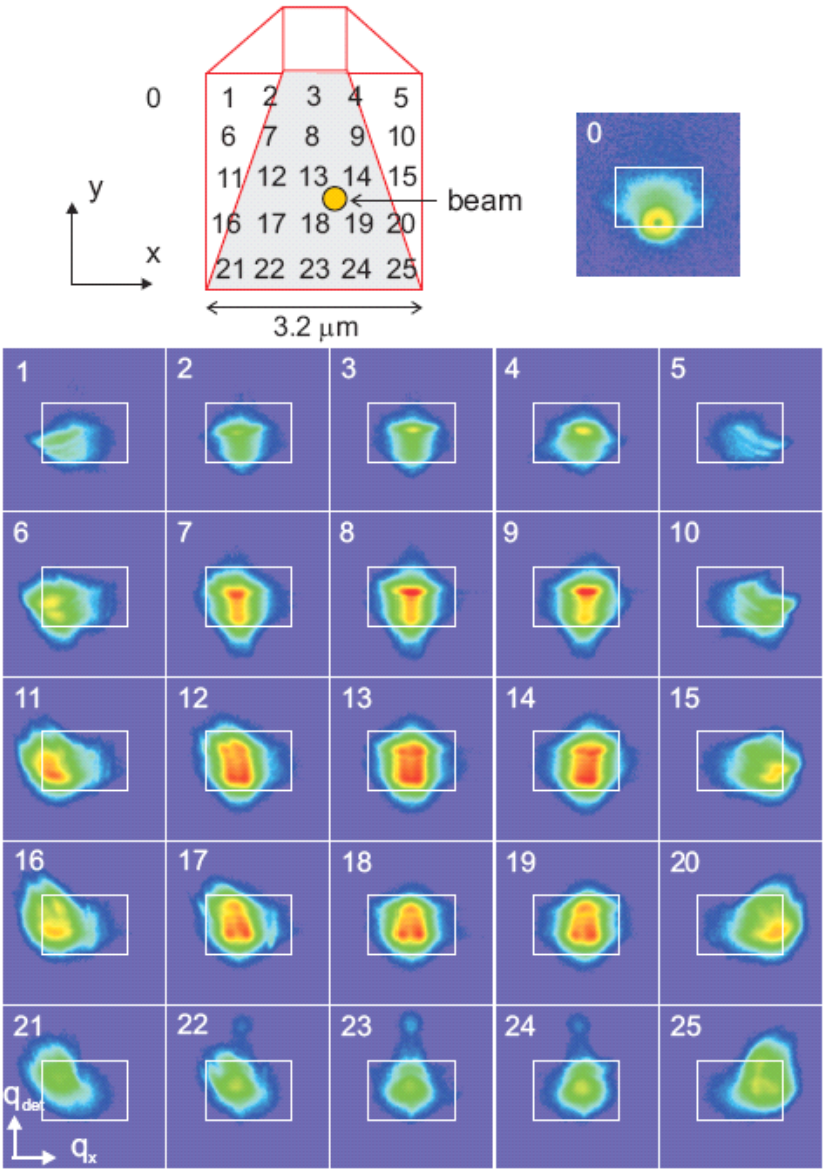

Figure 6. (from ref. [76] Diaz et al. with permission N° 3594481209644 John Wiley and Sons Inc.) Scanning diffraction micrographs recorded with the area detector positioned to record an image like the one shown in Figure 5f. Frames 1 to 25 correspond to the positions in real space sketched at the top part of the figure the size of the X-ray beam is also illustrated. Frame 0 is measured outside the island.

Another use of the coherence of the X-rays, and combined with the use of small X-ray spots (focusing) is done in a Coherent Diffraction Imaging (CDI) experiment. We show hereafter an example of studying individual SiGe islands [92]. Note also the retrieval of the strain inside the Si substrate, just beneath the SiGe island (Figure 7). Indeed, the measurement of the scattered intensity close to the Si substrate peak shows as well a certain distribution of the intensity in the Bragg peak. Also, it is possible to reconstruct (propagate) the X-ray wavefront (see for example [93] and references therein) and use the proper illumination function as input in the computing algorithms used to reconstruct the shape (density) and strain inside the investigated object.

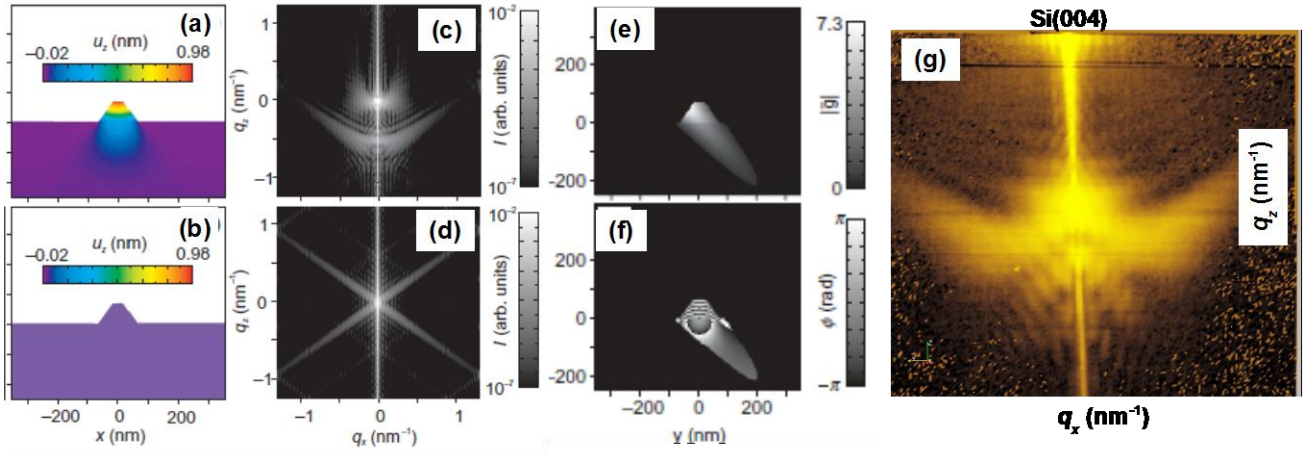

Figure 7. (from ref. [92] Diaz et al. with permission of © IOP Publishing & Deutsche Physikalische Gesellschaft. CC BY-NC-SA) Comparison of strain distribution (a, b) and scattered intensity (c, d) close to the (004) Bragg peak between strained (top) and unstrained (bottom) single SiGe island. (e, f) example of a 2D phase retrieval with a finite illumination function: reconstructed amplitude (e) and phase (f). (g) example of 2D data (logarithmic intensity scale) measured in the vicinity of Si(004) Bragg peak, for a single SiGe island using a coherent focused X-ray beam.

More complex systems, and especially more close to applications, can also be investigated: the technique is non-destructive for such types of samples (semiconductors). We illustrate this via the example of the investigation of a functioning metal-oxide-semiconductor field effect transistor MOSFET [2,18]. Indeed, tensile or compressive strain can be applied to the silicon channels of MOSFETs (depending if n- or p-type, respectively) in order to speed them up. One proposed concept is to use a SiGe island positioned below the channel of a Si based transistor, to act as a stressor element [2,158,169]. By using a hard X-ray focused beam, it is possible to locally measure the stress in such an object even after electrical connection, thus assimilated to a functioning device.

One approach which will be detailed hereafter is the combination of µXRD with an Atomic Force Microscope (AFM). This opens access to investigate in situ the mechanical properties of small individual objects when the micro and nano scale are approached. The XRD can give access to the strain inside the object with extremely good precision. The aim is to mechanically interact with a single small size object, which is in the same time characterized using µXRD technique. The lateral resolution in the XRD experiment should be good enough to ensure that the measured signal originates only from the object of interest, or parts of it. For this purpose, a specially designed AFM is mounted on the diffractometer [97,170–172]. A focused X-ray beam is used as a local probe. The sample can be imaged both using the X-ray spot (and XRD contrast) or with the AFM tip. This procedure allows positioning the AFM tip above the object of interest and the X-ray beam to illuminate precisely the very same object [159,171] .By performing XRD RSM and corresponding modelling, the strain inside the object is modelled and accessed (Figure 8) *via* direct comparison with the measured data [171]. Mechanical properties when the nanoscale is approached are thus accessed.

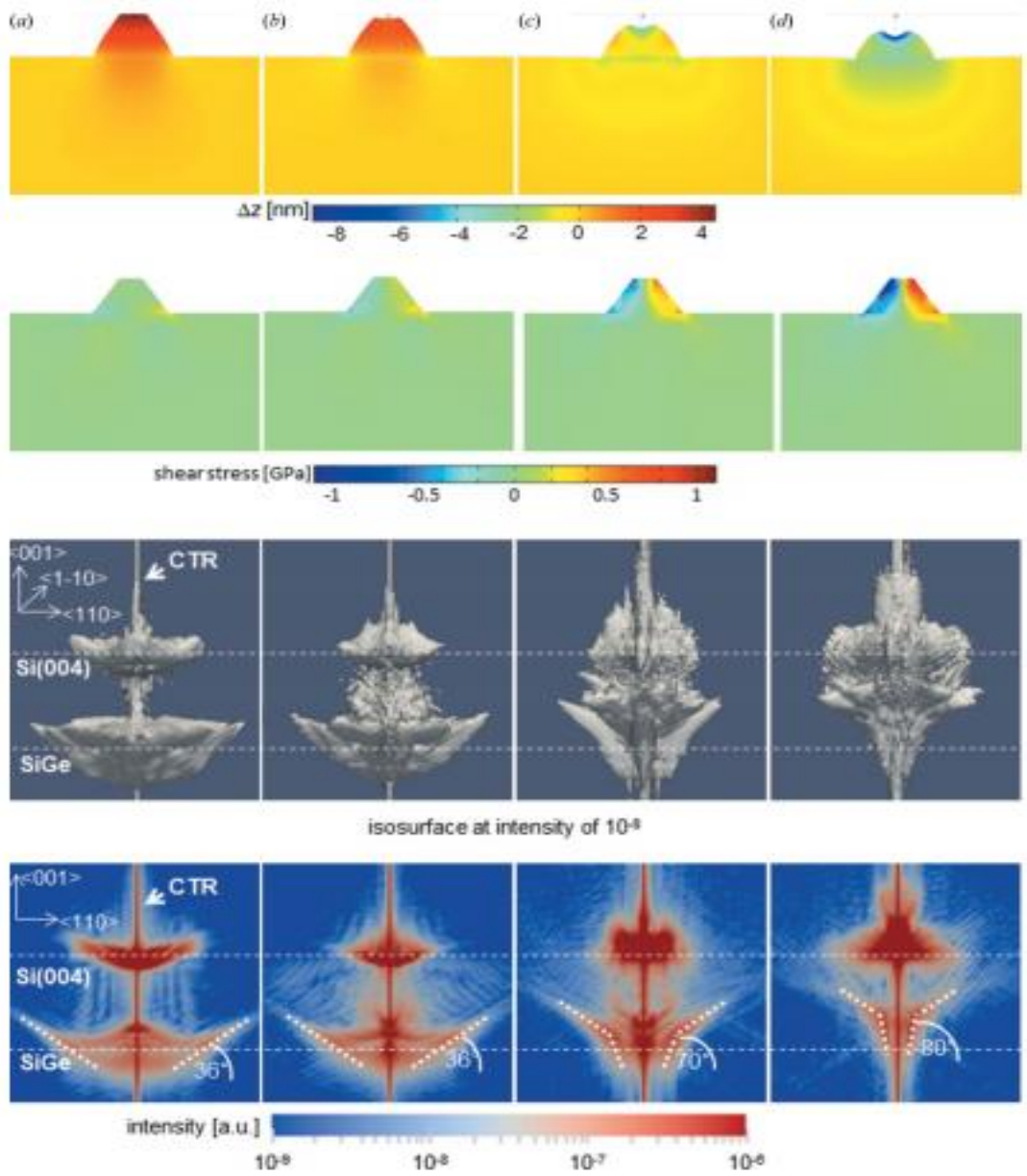

Figure 8. (from ref. [171] Cornelius et al., with permission IUCr http://dx.doi.org/10.1107/S0909049512023758) Displacement field (upper row) and shear stress (second row) simulated by the finite element method using COMSOL's multiphysics, 3D RSMs calculated from the displacement fields by fast Fourier transform (third row) and (qx, qz) cuts through the calculated 3D-RSMs at central qy (forth row) for (a) a SiGe island epitaxially grown on Si(001) and for samples with a distribution load of (b) 1GPa, (c) 3 GPa and (d) 5 GPa applied on the island top facet. The position of the Si(004) Bragg reflection and the signal of the SiGe island are indicated by dashed lines. The dotted lines highlight the Crystal Truncation Rods (CTRs) originating from the island side facets.

4. Conclusion

The development of state of the art hard X-ray spectro-microscopy techniques opens a way towards the characterization of the investigated samples at some nanometers spatial resolution with high elemental and chemical sensitivity. Advanced scanning hard X-ray nanoprobe techniques provide powerful tools for probing heterogeneous, complex systems down to the nanometer scales with high elemental and structural sensitivity, including dedicated beam-lines and nano-probe set-ups for material science applications [22,40,24,173–175] aiming also *in situ* and *in operando* studies [25]. X-ray nanoprobes providing 3D tomography [24,176–178] possibilities are emerging and provide access to the study of internal sample characteristics in a non-invasive way.

A strong need is evolving for the combination of more than one technique, in such a manner that the strengths of one complement the weaknesses of others. For example, the complementarity of X-ray methods and high resolution laboratory techniques (TEM, SEM, Raman spectroscopy [179], scanning probe microscopes [97,171,172,179] in probing locally the average composition with complementary spatial resolution and elemental sensitivity, is exploited by more and more combined utilization especially for the study of nano-structures. The synergy of different techniques together with the development of new approaches to their combined applications will allow the same nanoscale regions of material to be assessed in multiple microscopes in order to link directly and unambiguously structure and composition, to electrical and/or optical properties with high spatial resolution and high analytical sensitivity [180]. This would provide more complete picture than has been achieved so far.

A new challenge is to perform statistically meaningful investigations in order to bridge the gap between nano-characteristics and device functioning and properties and to make meaningful conclusion on the effect of nano-sized characteristics on that of the bulk sample. Characterizing material structures and compositions on various hierarchical length scales, from the engineering level down to the nanoscale, is of fundamental interest [25,179,181]. Characterizing with down to nanometer lateral resolution is not anymore the only requirement—rapid and reliable acquired data are demanded in order to be able to accurately extract information over large (several mm or cm) areas of the sample, while still having sub-μm down to nm lateral resolution.

This was lately addressed by several groups by implementing recently developed fast acquisition approaches; we will point out here some of them, which are introducing the concept [54,55,79,182,183,144,145,45]. In very simple terms, the idea behind is to acquire large sets of data (e.g. mapping large volumes of the reciprocal space, acquiring large raster maps with high resolution and several probed signals in the direct space, etc.) in extremely short time intervals, while still keeping the good data quality. We can mention some of the features which lead to the need and the development of such approaches:

i) The development of fast, low noise and low background, high dynamics and large surface area detectors: in a single image shot, wider regions of the space are covered while recording the signal, with high frequency sampling rates (>100 Hz).

ii) Higher photon density in the focused X-ray beams: this allows shortening the necessarily exposure time, while still having a good statistics of the data in the measured signal.

iii) Smaller size X-ray spots: this allows probing smaller and smaller volumes (lateral dimensions) in the samples. The number of sampling points in raster maps can be increased to address sample features at various lateral length scales, from nm to cm, resulting into imaging large

areas of the sample with very good lateral resolution. Zooming onto details can be performed then directly on the recorded data. Micro-, meso- and macro-scale characteristics can be thus accessed in a single measurement.

iv) Performing experiments involving fast phenomena (ex. transient phase transformation, thermal annealing,…): the fast acquisitions allow describing kinetics; the process is "cut" into snapshots which are then reconstructed into movies. In situ and operando measurements are clearly benefiting of these approaches.

v) Performing simultaneously, on the very same sample and under the very same experimental conditions, several analyses: it involves the use of several detectors which will acquire the data synchronously. We will point out here also an issue not always straightforward to deal with: in a lot of microbeam experiments, on the same sample, the acquisition time (statistics of the signal) can highly depend on the type of analysis technique used (particularly here XRF, XAS and XRD—it can be, for example, that a sample exhibits good crystallinity (i.e. short exposure times needed for XRD) but presence of traces of chemical elements (i.e. larger acquisition per point needed for XRF)). High detector sensitivity and dynamics can partially overcome this point. Fast acquisition schemes can also allow, in particular cases, performing subsequently the acquisition of the 2 datasets, thus minimizing a possible sample change (evolution) in between.

vi) Recording in reasonable time large and complete sets of data (e.g. mapping large regions of the the reciprocal space).

High flux to be provided by diffraction limited synchrotron sources and the related high intensity nano-beamlines will also contribute to such statistically meaningful and hierarchical length-scale measurements in a significant way. Next to third generation synchrotron sources (APS, DESY, Spring 8, ESRF, Soleil, Diamond, Alba, SLS etc.) new low emittance sources are already under construction (NSLS-II, MAX-IV, Sirius) (http://www.lightsources.org/regions). The fourth generation sources (MAX-IV in Sweden, Sirius in Brazil) make use of the significant improvement in accelerator technology enabling a radical increase in the horizontal emittance in order to approach the diffraction limit for multi-keV photons [184]. The upgrade of several synchrotrons worldwide is under design or consideration to achieve such diffraction limited storage rings (DLSR) [185]. These will open up experimental capabilities not possible right now in the field of hard X-ray spectromicroscopy and scanning imaging due to the large transversely coherent spectral flux for multi-keV photons. Diffraction-limited nano-focusing will largely benefit from this. Since the intensity in the diffraction-limited spot is given by the coherent flux provided by the source, these new highly coherent X-ray sources will permit several order higher flux density in the focused beam. Moreover, the almost round photon beam will be an additional asset for imaging applications, since e.g. the source can be directly de-magnified into a symmetric nano-beam without using a secondary source.

These future improvements of synchrotron sources must be followed by upgrade of optics, beamline technology, detectors and data analysis in order to fully profit from the new source characteristics. High optical quality optics is crucial to preserve the wave front of the highly coherent X-ray beams of the forthcoming low emittance sources. It is expected that nano-focusing optics, which are already approaching or overcoming the 10 nm spatial resolution limit [186–190] will become available with some nm's focal spot sizes for routine applications [191]. For example, the Hard X-ray Nanoprobe (HXN) beamline at NSLS-II [174] has a target of achieving a 1 nm spot size and as such it is a good marker for the transition to the expected DLSR performances. The resulting

intense diffraction limited size beams will open new perspectives for example in 3D tomography [24,176–178] and will make possible even 4D measurements e.g. XANES or time resolved tomography with some nm's spatial resolution within some tens of minutes [146]. However, the small focal distance (~mm) and focal depth (~μm) of nm resolution hard X-ray focusing optics might represent a technical challenge for practical applications, especially in case of in operando studies with dedicated sample environments or 3D tomography of several μm's thick samples. The latter might be overcome by new measurement methods and reconstruction techniques. Coherence based experimental techniques, such as coherent scatter imaging / ptychography, will highly profit from these source upgrades; next to the possibility of improving the spatial resolution down to some nm's in 3D [192], they will be extendable to higher energies compared to the <10 keV energies they are mostly used today.

As such, new diffraction limited synchrotron sources will complement free electron lasers (FEL), which are providing ultrashort femtosecond pulses with high peak brilliance and fully coherent beams. They are available also in the hard X-ray range for users since a little over five years (LCLS at SLAC National Accelerator Laboratory, SPring-8 Angstrom Compact Free Electron Laser, SACLA) and other ones are under construction (i.e European XFEL in Germany). FEL is expected to be the major experimental tool in areas of science, such as light–matter interactions, ultrafast time-resolved and single shot measurements at high spatial resolution, and study of matter under extreme conditions. We refer to the special issue of the Journal of Synchrotron Radiation covering the recent possibilities of FELS [193], as this is not the scope of the recent review.

High X-ray nano-beam intensities might create radiation damage even in hard condensed matter samples (which are, most of the time, considered as radiation resistant in X-rays) and related devices altering the studied characteristics and device performances [18,21]. Radiation damage is predicted to ultimately limit the achievable spatial resolution in many systems, particularly polymeric or soft matter, which have much lower critical doses for radiation damage than metal or semiconductor systems. This should be identified and minimized in a critical manner, though the quantification of radiation damage is not obvious. Performing rapid data acquisition can be one way to limit the dose deposited in the sample during the measurement. For this the development of high efficiency, low noise and large collection angle detectors are crucial.

All these issues make that the amount of acquired data in one experiment is tremendously increasing in size,and it is expected to lead to ~10 TB data volumes per experiment at new DLSR's. New algorithm of quantification, dose efficient measurement and statistically meaningful data exploitation are the challenges to be faced for efficient user-friendly operation possibilities. The data management (during and after the experimental campaign) is to be thoroughly considered. This comprises not only the data transfer and storage, but, in a more general manner, its handling. Combination and interpretation of large volumes of data (big data) originating from fast, multimodal and "multi-microscopy" measurements is a real challenge where on-line data visualization and fast data pre-treatment is becoming crucial for the success of an experiment.

During the fast acquisition, (pre-) visualization tools are required as diagnosis tools for the well advancing of the acquisition process itself: most of the time, it is useless to perform the acquisition of the dataset in times as short as seconds or below, if the experimentalist has no fast feedback (e.g. is data statistics good enough; is the region of interest to be mapped properly chosen, are there any changes visible if kinetics is measured, etc.) for decision about the continuation of the measurement. Achieving data exploitation times compatible (or at least of the same order of magnitude) with the

data acquisition times became a must lately [183] this can be mandatory for the well and optimum performing of an experiment, as well for the proper decision taken in how to conduct the experiment (for example, temperature annealing, better statistics or improved resolution, changing / adapting the sample environment, etc.).

Even the subsequent step, the thorough data exploiting, has to be carefully evaluated before performing it. Extracting the meaningful information, data correction and modelling might not be trivial at all. Even if the corresponding algorithms exist for "classical" acquisition schemes, they might simply not be adapted when dealing with very large datasets, as they can be extremely time consuming (e.g. ptychographic reconstruction, multivariate statistical analysis). Converting data from area detector images (e.g. powder diagrams extraction) are routinely done nowadays even at laboratory instruments for hundreds of images, but treating datasets (extraction, fitting, phase identification) of several 10^6 images or more, might become unrealistic in reasonable timeframes. Efforts are performed lately in developing or optimizing data treatment; quite often they involve an approach done "internally" (same group which did the data acquisition). The computer code optimization becomes very important. Sometimes, even a revision of the whole modelling process (and theory) should be desirable, if possible. It is clear that this should lead to some new approaches and understanding of the physical and chemical properties of such systems. Handling and exploitation of big data sets will need common effort among different establishments in data sharing and software developments and even to adapt already existing approaches in other fields e.g at XFEL's, astronomy, geology, meteorology, if possible.

We will point out two tools which can be used at present to exploit large datasets (10^6 datapoints or more) originating from XRF and/or XRD fast acquistion experiments: PyMCA [194] and PyFAI [195] respectively. The perfromances will highly depend on the computing configuration used. PyMCA can ensure pre-visualisation (for example by calculating, from the fluorescence raster maps, the specific Region of Interest (ROI) contrast maps) rather quickly once the data is loaded. This might be enough for defining areas of interest in the sample, especially if isolated chemical species are present (no XRF signal superposition). In reverse, a proper deconvolution of all the XRF spectra of a 10^6 raster map can take up to several days. Concerning PyFAI, a computational performance of up to 300 frames per second (images of 1 Mega-pixels each) was reporteed [195].

These developments will provide breakthrough in high-resolution imaging and tomography, microscopy, and spectroscopy. New techniques and approaches will provide new perspectives for high societal impact studies in material sciences and the related engineering and fabrication process.

Conflict of Interest

The authors declare that there are no conflicts of interest related to this study.

References

1. Bordiga S, Groppo E, Agostini G, et al. (2013) Reactivity of surface species in heterogeneous catalysts probed by in situ x-ray absorption techniques. *Chem Rev* 113: 1736–1850.
2. Hrauda N, Zhang J, Wintersberger E, et al. (2011) X-ray Nanodiffraction on a Single SiGe Quantum Dot inside a Functioning Field-Effect Transistor. *Nano Lett* 11: 2875–2880.

3. Buurmans ILC, Weckhuysen BM (2012). Space and time as monitored by spectroscopy, Nature Chemistry 4:873–886.
4. Hitchcock AP, Johansson GA, Mitchell GH, et al. (2008). 3-d chemical imaging using angle-scan nanotomography in a soft X-ray scanning transmission X-ray microscope. *Appl Phys A* 92:447–452.
5. Hitchcock AP (2012) Soft X-Ray Imaging and Spectromicroscopy, in Handbook of Nanoscopy, Volume 1&2 (eds G. Van Tendeloo, D. Van Dyck and S. J. Pennycook), Wiley-VCH Verlag GmbH & Co. KGaA, Weinheim, Germany.
6. Ade H, Stoll H (2009) Near-edge X-ray absorption fine-structure microscopy of organic and magnetic materials. *Nature Materials* 8: 281–290.
7. Kaulich B, Thibault P, Gianoncelli A, et al. (2011) Transmission and emission x-ray microscopy: operation modes, contrast mechanisms and applications. *J Phys Cond Matter* 23: 083002.
8. Beale AM, Jacques SDM, & Weckhuysen BM (2010). In-situ characterization of heterogeneous catalysts themed issue Chemical imaging of catalytic solids with synchrotron radiation. *Chem Soc Rev* 39: 4656–4672.
9. Harris WM, Nelson GJ, Kiss A, at al. (2012) Nondestructive volumetric 3-D chemical mapping of nickel-sulfur compounds at the nanoscale. *Nanoscale* 4: 1557–1560.
10. Wang J, Chen-wiegart YK, Wang J, (2014) In operando tracking phase transformation evolution of lithium iron phosphate with hard X-ray microscopy. *Nature Com* 5: 1.
11. Fenter P, Park C, Zhang Z, et al. (2006) Observation of Sub-nm-High Surface Topography with X-ray Reflection Phase-Contrast Microscopy. *Nat Phys* 2: 700–704.
12. Fenter P, Park C, Kohli V, et al. (2008) Image contrast in X-ray reflection interface microscopy: comparison of data with model calculations and simulations. *J Synch Rad* 15: 558–571.
13. Fister TT, Goldman JL, Long BR, et al. (2013) X-ray diffraction microscopy of lithiated silicon microstructures. *Appl Phys Lett* 102: 131903.
14. Hilhorst J, Marschall F, Tran Thi TN, et al. (2014) Full-field X-ray diffraction microscopy using polymeric compound refractive lenses. *J Appl Cryst* 47: 1882–1888.
15. Mocuta C, Barbier A, Stanescu S, et al. (2013) X-ray diffraction imaging of metal–oxide epitaxial tunnel junctions made by optical lithography: use of focused and unfocused X-ray beams. *J Synch Rad* 20: 355–365.
16. Luebbert D, Baumbach T, Hartwig J, et al. (2000) μm-resolved high resolution X-ray diffraction imaging for semiconductor quality control. *Nucl Meth Phys Res B*160:521–527.
17. Ice GE, Budai JD, Pang JWL (2011) The Race to X-ray Microbeam and Nanobeam Science. *Science* 334: 1234–1239.
18. Stangl J, Mocuta C, Chamard V, et al. (2014) Nanobeam X-ray Scattering—Probing matter at the Nanoscale. Wiley VCH WileyBook.
19. Johannes A, Noack SJrWP, Kumar S, et al. (2014) Enhanced sputtering and incorporation of Mn in implanted GaAs and ZnO nanowires. *J Phys D Appl Phys* 47: 394003.
20. Segura-Ruiz J, Martinez-Criado G, Chu MH, et al. (2013) Synchrotron nanoimaging of single In-rich InGaN nanowires. *J Appl Phys* 113: 136511.
21. Stangl J, Mocuta C, Diaz A, et al. (2009) X-Ray Diffraction as a Local Probe Tool. *Chem Phys Chem* 10: 2923–2930.
22. Maser J, Lai B, Buonassisi T, et al. (2014) A Next-Generation Hard X-Ray Nanoprobe Beamline for In Situ Studies of Energy Materials and Devices. *Metall Mater Trans A* 45: 85–97.

23. Martinez-Criado G, Segura-Ruiz J, Alén B, et al. (2014) Exploring single semiconductor nanowires with a multimodal hard X-ray nanoprobe. *Adv Mater* 1–7.
24. Holt M, Harder R, Winarski R, et al. (2013) Nanoscale Hard X-ray Microscopy Methods for Materials Studies. *Annu Rev Mater Res* 43: 3.1–3.29.
25. Weker JN, Toney MF (2015) Emerging In Situ and Operando Nanoscale X-Ray Imaging Techniques for Energy Storage Materials. *Adv Func Mat* 25: 1622–1637.
26. Sirenko AA, Reynolds CL, Peticolas LJ, et al. (2003) Micro-X-ray fluorescence and micro-photoluminescence in InGaAsP and InGaAs layers obtained by selective area growth. *J Crystal Growth* 253: 38–45.
27. Mino L, Agostino A, Codato S, et al. (2010) Study of epitaxial selective area growth In1-xGaxAs films by synchrotron μ-XRF mapping. *J Anal At Spectrom* 25: 831–836.
28. Buonassisi T, Istratov AA, Marcus MA, et al. (2005) Engineering metal-impurity nanodefects for low-cost solar cells. *Nature Materials* 4: 676–679.
29. Kwapil W, Gundel P, Schubert MC, et al. (2009) Observation of metal precipitates at prebreakdown sites in multicrystalline silicon solar cells. *Appl Phys Lett* 95:23–25.
30. Bertoni MI, Fenning DP, Rinio M, et al. (2011) Nanoprobe X-ray fluorescence characterization of defects in large-area solar cells. *Energy Environ Sci* 4: 4252–4257.
31. Hu Q, Aboustait M, Ley MT, et al. (2014) Combined three-dimensional structure and chemistry imaging with nanoscale resolution. *Acta Materialia* 77: 173–182.
32. Mino L, Agostini G, Borfecchia E, et al. (2013) Low-dimensional systems investigated by x-ray absorption spectroscopy: a selection of 2D, 1D and 0D cases. J Phys D: *Appl Phys* 46: 423001.
33. Martinez-Criado G, Segura-Ruiz J, Chu M, et al. (2014a) Crossed Ga2O3/SnO2 Multiwire Architecture: A Local Structure Study with Nanometer Resolution. *Nano Letters* 14: 5479–5487.
34. Larcheri S, Rocca F, Pailharey D, et al. (2009) A new tool for nanoscale X-ray absorption spectroscopy and element-specific SNOM microscopy. *Micron* 40: 61–65.
35. Shirato N, Cummings M, Kersell H, et al. (2014) Elemental Fingerprinting of Materials with Sensitivity at the Atomic Limit. *Nano Letters* 14: 6499–6504.
36. Mocuta C, Stangl J, Mundboth K, et al. (2008) Beyond the ensemble average: X-ray microdiffraction analysis of single SiGe islands. *Phys Rev B*77: 245425.
37. Bleuet P, Cloetens P, Gergaud P, et al. (2009) A hard x-ray nanoprobe for scanning and projection nanotomography. *Rev Sci Inst* 80: 056101.
38. Bunk O, Bech M, Jensen TH, et al. (2009) Multimodal x-ray scatter imaging. *New J Phys* 11: 123016.
39. Meirer F, Cabana J, Liu Y, et al. (2011) Three-dimensional imaging of chemical phase transformations at the nanoscale with full-field transmission X-ray microscopy. *J Synch Rad* 18: 773–781.
40. Villanova J, Segura-Ruiz J, Lafford T, et al. (2012) Synchrotron microanalysis techniques applied to potential photovoltaic materials. *J Sync Rad* 19: 521–524.
41. Gómez-Gómez M, Garro N, Segura-Ruiz J, et al. (2014) Spontaneous core–shell elemental distribution in In-rich InxGa1-xN nanowires grown by molecular beam epitaxy. *Nanotechnology* 25: 075705.
42. Tsuji K, Injuk J, Van Grieken R (2004) X-ray spectrometry: recent technological advances. John Wiley & Sons, Ltd.

43. Hippert F, Geissler E, Hodeau JL, et al. (eds) (2006) Neutron and X-ray spectroscopy. Springer.
44. Van Grieken R, Markowicz A (2001) Handbook of X-Ray Spectrometry. CRC Press.
45. Somogyi A, Medjoubi K, Baranton G, et al. (2015). Optical design and multi-length-scale scanning spectro-microscopy possibilities at the Nanoscopium beamline of Synchrotron Soleil. J Synch Rad. In press
46. Schroer CG (2001) Reconstructing x-ray fluorescence microtomograms. *Appl Phys Lett* 79: 1912.
47. Golosio B, Somogyi A, Simionovici A, et al. (2004) Nondestructive three-dimensional elemental microanalysis by combined helical x-ray microtomographies. *Appl Phys Lett* 84: 2199.
48. Bleuet P, Gergaud P, Lemelle L, et al. (2010) 3D chemical imaging based on a third-generation synchrotron source. *TrAC-Trends in Anal Chem* 29: 518–527.
49. De Jonge MD, Vogt S,(2010) Hard X-ray fluorescence tomography-an emerging tool for structural visualization. *Curr Opin Struct Biol* 20: 606.
50. Kak AC, Slaney M (2001) Principles of Computerized Tomographic Imaging. Philadelphia: Society for Industrial and Applied Mathematics.(an abridged republication of the work first published by IEEE Press, New York, 1988).
51. Golosio B, Simionovici A, Somogyi A, et al. (2003) Internal elemental microanalysis combining XRF, Compton and Transmission Tomography. *J Appl Phys* 94: 145.
52. Naghedolfeizi M, Chung J, Morris R, et al. (2003) X-ray fluorescence microtomography study of trace elements in a SiC nuclear fuel shell. *J Nucl Mater* 312: 146–155.
53. Lombi E, De Jonge MD, Donner E, et al. (2011) Fast X-ray fluorescence microtomography of hydrated biological samples. *PLoS ONE* 6: e20626.
54. Medjoubi K, Leclercq N, Langlois F, et al. (2013) Development of fast, simultaneous and multi-technique scanning hard X-ray microscopy at Synchrotron Soleil. *J Synch Rad* 20: 293–300.
55. Medjoubi K, Bonissent A, Leclercq N, et al. (2013) Simultaneous fast scanning XRF, dark field, phase-, and absorption contrast tomography. Proceedings of SPIE, 2013, 8851:art.n °88510P
56. Vincze L, Vekemans B, Brenker FE (2004) Three-Dimensional Trace Element Analysis by Confocal X-ray Microfluorescence Imaging. *Anal Chem* 76: 6786.
57. Lamberti C, Agostini G, (2013) Characterization of Semiconductor Heterostructures and Nanostructures 2nd edn, ed C Lamberti, G Agostini (Amsterdam: Elsevier).
58. Calvin S (2013) XAFS for Everyone. Boca Raton FL: Taylor and Francis.
59. Schnohr CS, Ridgway MC (Eds.) (2015) X-Ray Absorption Spectroscopy of semiconductors, Series: Springer Series in Optical Sciences, Vol. 190 (Springer)
60. Martinez-Criado G, Somogyi A, Homs A, et al. (2005a) Micro-x-ray absorption near-edge structure imaging for detecting metallic Mn in GaN. *Appl Phys Lett* 87: 061913.
61. Seifert W, Vyvenko O, Arguirov T, et al. (2009) Synchrotron-based investigation of iron precipitation in multicrystalline silicon. *Superlattice Microst* 45: 168–176.
62. Watts B, McNeil C (2010) Simultaneous Surface and Bulk Imaging of Polymer Blends with X-ray Spectromicroscopy. *Macromolec Rapid Commun* 31: 1706–1712.
63. Watts B, McNeil C, Raabe J (2012) Imaging nanostructures in organic Semiconductor films with scanning transmission X-ray spectro-microscopy. *Synthetic Met* 161: 2516–2520.

64. d'Acapito F (2015) Group III–V and II–VI Nanowires in X-Ray Absorption Spectroscopy of Semiconductors. *Springer Series in Optical Sciences* 190: 269–286.
65. Strachan JP, Medeiros-Ribeiro G, Yang JJ, et al. (2011) Spectromicroscopy of tantalum oxide memristors. *Appl Phys Lett* 98: 24–26.
66. Rau C, Somogyi A, Simionovici A (2003) Microimaging and tomography with chemical speciation. *Nucl Instr Methods Phys Res B* 200: 444–450.
67. Segura-Ruiz J, Martinez-Criado G, Chu MH, et al. (2011) Nano-X-ray Absorption Spectroscopy of Single Co-Implanted ZnO Nanowires. *Nano Letters* 11: 5322–5326.
68. Wang J, Chen-Wiegart YK, Wang J (2013) In situ chemical mapping of a lithium-ion battery using full-field hard X-ray spectroscopic imaging. *Chem Com* 49: 6480–6482.
69. Rosenberg RA, Shenoy GK, Sun XH, et al. (2006) Time-resolved x-ray-excited optical luminescence characterization of one-dimensional Si—CdSe heterostructures. *Appl Phys Lett* 89: 243102.
70. O'Malley SM, Revesz P, Kazimirov A, et al. (2011) Time-resolved x-ray excited optical luminescence in InGaN / GaN multiple quantum well structures. *J Appl Phys* 109: 124906.
71. Bianconi A, Jackson D (1978) Intrinsic luminescence excitation spectrum and extended x-ray absorption fine structure above the K edge in CaF_2. *Phys Rev A* 17: 2021–2024.
72. Goulon J, Tola P, Lemonnier M, et al. (1983) On a site-selective EXAFS experiment using optical emission, Chem. Phys. 78: 347–356.
73. Rogalev A, & Goulon J (2002) X-ray excited optical luminescence spectroscopies, Advanced Series in Physical Chemistry: Volume 12, Chemical Applications of Synchrotron Radiation, Edited by: Sham TK, 707–760. World Scientific.
74. Sham TK, Naftel SJ, Kim PG, et al. (2004) Electronic structure and optical properties of silicon nanowires : A study using x-ray excited optical luminescence and x-ray emission spectroscopy, Phys Rev B70:045313.
75. Hanke M, Dubslaff M, Schmidbauer M, et al. (2008) Scanning x-ray diffraction with 200 nm spatial resolution. *Appl Phys Lett* 92: 193109.
76. Diaz A, Mocuta C, Stangl J, et al. (2009) Spatially resolved strain within a single SiGe island investigated by X-ray scanning microdiffraction. *Phys Stat Sol A* 206: 1829–1832.
77. Mocuta C, Barbier A, Ramos AV, et al. (2007) Effect of optical lithography patterning on the crystalline structure of tunnel junctions. *Appl Phys Lett* 91: 241917.
78. Evans PG, Savage DE, Prance JR, et al. (2012) Nanoscale Distortions of Si Quantum Wells in Si/SiGe Quantum-Electronic Heterostructures. *Adv Mater* 24: 5217–5221.
79. Chahine GA, Richard MI, Homs-Regojo RA, et al. (2014) Imaging of strain and lattice orientation by quick scanning X-ray microscopy combined with three dimensional reciprocal space mapping. *J Appl Cryst* 47: 762–769.
80. Goodman JW (2005) Introduction to Fourier Optics, Roberts and Company Publishers
81. Garcia-Sucerquia J, Xu W, Jericho SK, et al. (2006) Digital in-line holographic microscopy. *Appl Opt* 45: 836–850.
82. Leith EN, Upatniesks J (1962) Reconstructed Wavefronts and Communication Theory. *J Opt Soc Am* 52: 1123–1128.
83. Fuhse C, Ollinger C, Saldit T (2006) Waveguide-Based Off-Axis Holography with Hard X Rays. *Phys Rev Lett* 97: 254801.

84. Eisebitt S, Luning J, Schlotter WF, et al. (2004) Lensless imaging of magnetic nanostructures by X-ray spectro-holography. *Nature* 432: 885–888.
85. Stadler LM, Gutt C, Autenrieth T, et al. (2008) Hard X Ray Holographic Diffraction Imaging. *Phys Rev Lett* 100: 245503.
86. Chamard V, Stangl J, Carbone D, et al. (2010) Three-Dimensional X-Ray Fourier Transform Holograhpy: The Bragg Case. *Phys Rev Lett* 104: 165501.
87. Livet F (2007) Diffraction with a coherent X-ray beam: dynamics and imaging. *Acta Crystallogr A* 63: 87–107.
88. Miao J, Charalambous P, Kirz J, et al. (1999) Extending the methodology of X-ray crystallography to allow imaging of micrometre-sized non-crystalline specimens. *Nature* 400: 342–344.
89. Miao J, Ishikawa T, Johnson B, et al. (2002) High Resolution 3D X-Ray Diffraction Microscopy. *Phys Rev Lett* 89: 088303.
90. Takahashi T, Zettsu N, Nishino Y, et al. (2010) Three-Dimensional Electron Density Mapping of Shape-Controlled Nanoparticle by Focused Hard X-ray Diffraction Microscopy. *Nano Lett* 10: 1922–1926.
91. Diaz A, Mocuta C, Stangl J, et al. (2009B) Coherent diffraction imaging of a single epitaxial InAs nanowire using a focused x-ray beam. *Phys Rev B* 79: 125324.
92. Diaz A, Chamard V, Mocuta C, et al. (2010) Imaging the displacement field within epitaxial nanostructures by coherent diffraction: a feasibility study. *New J Phys* 12: 035006.
93. Mastropietro F, Carbone D, Diaz A, et al. (2011) Coherent x-ray wavefront reconstruction of a partially illuminated Fresnel zone plate. *Opt Express* 19: 19223–19232.
94. Pfeiffer M, Williams GJ, Vartanyants IA, et al. (2006) Three-dimensional mapping of a deformation field inside a nanocrystal. *Nature* 442: 63–66.
95. Robinson IK, Vartanyants IA, Williams GJ, et al. (2001) Reconstruction of the Shapes of Gold Nanocrystals Using Coherent X-Ray Diffraction. *Phys Rev Lett* 87: 195505.
96. Newton MC, Leake SJ, Harder R, et al. (2010) Three-dimensional imaging of strain in a single ZnO nanorod. *Nature Mater* 9: 120–124.
97. Beutier G, Verdier M, Parry G, et al. (2013). Strain inhomogeneity in copper islands probed by coherent X-ray diffraction. *Thin Solid Films* 530: 120–124.
98. Minkevich AA, Gailhanou M, Micha JS, et al. (2007) Inversion of the Diffraction Pattern from an Inhomogeneously Strained Crystal using an Iterative Algorithm. *Phys Rev B* 76: 104106.
99. Minkevich AA, Baumbach T, Gailhanou M, et al. (2008) Applicability of an iterative inversion algorithm to the diffraction patterns from inhomogeneously strained crystals. *Phys Rev B* 78: 174110.
100. Minkevich AA, Fohtung E, Slobodskyy T, et al. (2011) Strain field in (Ga,Mn)As/GaAs periodic wires revealed by coherent X-ray diffraction. *European Phys Lett* 94: 66001.
101. Williams GJ, Quiney HM, Dhal BB, et al. (2006) Fresnel Coherent Diffractive Imaging. *Phys Rev Lett* 97: 025506.
102. Quiney HM, Peele AG, Cai Z, et al. (2006) Diffractive imaging of highly focused X-ray fields. *Nature Phys* 2: 101–104.
103. Faulkner HLM, Rodenberg JM (2004) Movable Aperture Lensless Transmission Microscopy: A Novel Phase Retrieval Algorithm. *Phys Rev Lett* 93: 023903.

104. Bunk O, Dierloff M, Kynde S, et al. (2007) Influence of the overlap parameter on the convergence of the ptychographical iterative engine. *Ultramicroscopy* 108: 481–487.
105. Maiden A, Rodenburg J (2009) An improved ptychographical phase retrieval algorithm for diffractive imaging. *Ultramicroscopy* 109: 1256–1262.
106. Guizar-Sicairos M, Fineup J (2008) Phase retrieval with transverse translation diversity: a nonlinear optimization approach. *Opt Express* 16: 7264–7278.
107. Dierolf M, Menzel A, Thibault P, et al. (2010) Ptychographic X-ray computed tomography at the nanoscale. *Nature* 467: 436–439.
108. Godard P, Carbone G, Allain M, et al. (2011) Three-dimensional high-resolution quantitative microscopy of extended crystals. *Nature Commun* 2: 568.
109. Godard P, Allain M, Chamard V, et al. (2011B) Imaging of highly inhomogeneous strain field in nanocrystals using x-ray Bragg ptychography: A numerical study. *Phys Rev B* 84: 144109.
110. Korsunsky A, Hofmann F, Abbey B, et al. (2012) Analysis of the internal structure and lattice (mis) orientation in individual grains of deformed CP nickel polycrystals by synchrotron X-ray micro-diffraction and microscopy. *Int J Fatigue* 42: 1–13.
111. Georgiadis M, Guizar-sicairos M, Zwahlen A, et al. (2015).3D scanning SAXS: A novel method for the assessment of bone ultrastructure orientation. *Bone* 71: 42–52.
112. Snigirev A, Snigireva I, Kohn V, et al. (1995) On the possibilities of x-ray phase contrast microimaging by coherent high‐energy synchrotron radiation. *Rev Sci Instrum* 66: 5486.
113. Cloetens P, Pateyron-Salomé M, Buffière J, et al. (1997) Observation of microstructure and damage in materials by phase sensitive radiography and tomography. *J Appl Phys* 81: 5.
114. Pfeiffer M, Bech M, Bunk O, et al. (2008) Hard-X-ray dark-field imaging using a grating interferometer. *Nature Mater* 7: 134–137.
115. Weitkamp T, Diaz A, David C, et al. (2005) X-ray phase imaging with a grating interferometer. *Opt Express* 13: 6296.
116. David C, Nohammer B, Solak H, et al. (2002) Differential x-ray phase contrast imaging using a shearing interferometer. *Appl Phys Lett* 81: 3287.
117. Egan CK, Wilson MD, Veale MC, et al. (2014) Material specific X-ray imaging using an energy-dispersive pixel detector. *Nucl Instrum Meth Phys Res B* 324: 25–28.
118. Ice GE, Specht ED (2012) Microbeam, timing and signal-resolved studies of nuclear materials with synchrotron X-ray sources. *J Nucl Mat* 425: 233–237.
119. Singer A, Ulvestad A, Cho H, et al. (2014) Nonequilibrium Structural Dynamics of Nanoparticles in LiNi1/2Mn3/2O4 Cathode under Operando Conditions. *Nano Lett* 14: 5295–5300.
120. Wang L, Ding Y, Patel U, et al. (2011) Studying single nanocrystals under high pressure using an x-ray nanoprobe. *Rev Sci Inst* 82: 43903.
121. Xu F, Helfen L, Suhonen H, et al. (2012) Correlative Nanoscale 3D Imaging of Structure and Composition in Extended Objects. *PLOS One* 7: e50124.
122. McHugo S, Thompson C, Périchaud I, et al. (1998) Direct correlation of transition metal impurities and minority carrier recombination in multicrystalline silicon. *Appl Phys Lett* 72: 3482.
123. Vyvenko OF, Buonassisi T, Istratov AA, et al. (2002) X-ray beam induced current—A synchrotron radiation based technique for the in situ analysis of recombination properties and chemical nature of metal clusters in silicon. *J Appl Phys* 91: 3614–3617.

124. Istratov AA, Buonassisi T, McDonald RJ, et al. (2003) Metal content of multicrystalline silicon for solar cells and its impact on minority carrier diffusion length. *J Appl Phys* 94: 6552.
125. Buonassisi T, Istratov AA, Huer M, et al. (2005a) Synchrotron-based investigations of the nature and impact of iron contamination in multicrystalline silicon solar cells. *J Appl Phys* 97: 074901.
126. Buonassisi T, Istratov AA, Pickett MD, et al. (2006) Chemical natures and distributions of metal impurities in multicrystalline silicon materials. Progress in Photovoltaics: *Res App* 14: 512–531.
127. Trushin M, Seifert W, Vyvenko O, et al. (2010) XBIC/μ-XRF/μ-XAS analysis of metals precipitation in block-cast solar silicon. *Nucl Inst Methods Phys Res B* 268: 254–258.
128. Gundel P, Schubert MC, Heinz FD, et al. (2010) Impact of stress on the recombination at metal precipitates in silicon. *J Appl Phys* 108: 103707.
129. Fenning DP, Hofstetter J, Bertoni MI, et al. (2011) Iron distribution in silicon after solar cell processing: Synchrotron analysis and predictive modeling. *Appl Phys Lett* 98: 162103.
130. Fenning DP, Hofstetter J, Bertoni MI, et al. (2013). Precipitated iron: A limit on gettering efficacy in multicrystalline silicon Precip. *J Appl Phys* 113: 044521.
131. Zuschlag M, Schwab M, Merhof D, Hahn G (2014) Transition metal precipitates in mc Si: a new detection method using 3D-FIB. *Solid State Phenom* 205–206: 136–141.
132. Dietl T (2010) A ten-year perspective on dilute magnetic semiconductors and oxides. *Nat Mater* 9: 965–974.
133. Martinez-Criado G, Somogyi A, Ramos S, et al. (2005) Mn-rich clusters in GaN: Hexagonal or cubic symmetry? *Appl Phys Lett* 86: 131927.
134. Mart ńez-Criado G, Somogyi A, Hermann M, et al. (2004) Direct observation of Mn clusters in GaN by X-ray scanning microscopy. *Jap J Appl Phys Part 2: Letter* 43: 695–697.
135. Sancho-Juan O, Cantarero A, Mart ńez-Criado G, et al. (2006) X-ray absorption near edge spectroscopy at the Mn K-edge in highly homogeneous GaMnN diluted magnetic semiconductors. *Physica Status Solidi (B) Basic Res* 243: 1692–1695.
136. Sancho-Juan O, Cantarero A, Garro N, et al. (2009) X-ray absorption near-edge structure of GaN with high Mn concentration grown on SiC. *J Phys Cond Mat* 21: 295801.
137. Farvid SS, Hegde M, Hosein ID, et al. (2011) Electronic structure and magnetism of Mn dopants in GaN nanowires : Ensemble vs single nanowire measurements. *Appl Phys Lett* 99: 222504.
138. Segura-Ruiz J, Martinez-Criado G, Denker C, et al. (2014) Phase Separation in Single InxGa1-xN Nanowires Revealed through a Hard X ray Synchrotron Nanoprobe. *Nano Lett* 14: 1300–1305.
139. Egerton RF, Li P, Malac M (2004) Radiation damage in the TEM and SEM, 35: 399–409.
140. Hitchcock AP, Dynes JJ, Johansson G, et al. (2008a) Comparison of NEXAFS microscopy and TEM-EELS for Studies of Soft Matter. *Micron* 39:741–748.
141. Harris WM, Lombardo JJ, Nelson GJ, et al. (2014) Three-dimensional microstructural imaging of sulfur poisoning-induced degradation in a Ni-YSZ anode of solid oxide fuel cells. *Scientific Reports* 4: 5246.
142. Martinez-Criado G, Alen B, Homs A, et al. (2006) Scanning x-ray excited optical luminescence microscopy in GaN. *Appl Phys Lett* 89: 221913.
143. Mart ńez-Criado G, Homs A, Al én B, et al. (2012) Probing quantum confinement within single core- multishell nanowires. *Nano Lett* 12: 5829–5834.

144. Paterson D, Jonge MD De, Howard DL, et al. (2011). The X-ray fluorescence microscopy beamline at the Australian synchrotron. *AIP Conf Proc* 1365:219–222.
145. Huang X, Lauer K, Clark JN, et al. (2015). Fly-scan ptychography. Scientific Reports 5:9074.
146. Jonge MD De, Ryan G, Jacobsen CJ (2014) X-ray nanoprobes and diffraction-limited storage rings : opportunities and challenges of fluorescence tomography of biological specimens. *J Synch Rad* 21:1031–1047.
147. Guillamet R, Lagay N, Mocuta C, et al. (2013) Micro-characterization and three imensional modeling of very large waveguide arrays by selective area growth for photonic integrated circuits. *J Cryst Growth* 370: 128–132.
148. Decobert J, Guillamet R, Mocuta C, et al. (2013) Structural characterization of selectively grown multilayers with new high angular resolution and sub-millimeter spot-size x-ray diffractometer. *J Cryst Growth* 370: 154–156.
149. Bussone G, Schäfer-Eberwein H, Dimakis E, et al. (2015) Correlation of Electrical and Structural Properties of Single As-Grown GaAs Nanowires on Si (111) Substrates. *Nano Lett* 15: 981.
150. Beutier G, Verdier M, De Boissieu M, et al. (2013b) Combined coherent x-ray micro-diffraction and local mechanical loading on copper nanocrystals. *J Phys Conf Series* 425: 132003.
151. Mondiali V, Bollani M, Cecchi S, et al. (2014A) Dislocation engineering in SiGe on periodic and aperiodic Si(001) templates studied by fast scanning X-ray nanodiffraction. *Appl Phys Lett* 104: 021918.
152. Mondiali V, Bollani M, Chrastina D, et al. (2014B) Strain release management in SiGe/Si films by substrate patterning. *Appl Phys Lett* 105: 242103.
153. Als-Nielsen J, McMorrow D (2011) Elements of Modern X-ray Physics. (2nd Edition), Wiley.
154. Riekel C, Davies JD (2005) Applications of synchrotron radiation micro-focus techniques to the study of polymer and biopolymer fibers. *Curr Opin Colloid In* 9: 396–403.
155. Larson BC, Yang W, Ice GE, et al. (2002) Three-dimensional X-ray structural microscopy with submicrometre resolution. *Nature* 415: 887–890.
156. Budai JD, Yang WG, Tamura N, et al. (2003) X-ray microdiffraction study of growth modes and crystallographic tilts in oxide films on metal substrates. *Nature Materials* 2: 487–492.
157. Schmidbauer M (2004) X-Ray Diffuse Scattering from Self-Organized Mesoscopic Semiconductor Structures. *Springer Tracts in Modern Physics* 199.
158. Hrauda N, Zhang JJ, Groiss H, et al. (2013) Strain relief and shape oscillations in site-controlled coherent SiGe islands. *Nanotechnology* 24: 335707.
159. Barbier A, Mocuta C, Belkhou R (2012) Selected Synchrotron Radiation Techniques, chapter in Enciclopedia of Nanotechnology. ed. B. Bhushan, 2322–2344. Springer.
160. Holy V, Mundboth K, Mocuta C, et al. (2008) Structural characterization of self-assembled semiconductor islands by three-dimensional X-ray diffraction mapping in reciprocal space. *Thin Solid Films* 516: 8022–8028.
161. Mocuta C, Barbier A, Ramos AV, et al. (2009) Crystalline structure of oxide-based epitaxial tunnel junctions. *Eur Phys J Special Topics* 167: 53–58.
162. Murray CE, Noyan IC, Mooney PM, et al. (2003) Mapping of strain fields about thin film structures using x-ray microdiffraction. *Appl Phys Lett* 83: 4163.
163. Murray CE, Saenger KL, Kalenci O, et al. (2008) Submicron mapping of silicon-on-insulator strain distributions induced by stressed liner structures. *J Appl Phys* 104: 013530.

164. Murray CE, Yan HF, Noyan IC, et al. (2005) High-resolution strain mapping in heteroepitaxial thin-film features. *J Appl Phys* 98: 013504.
165. Murray CE, Ying A, Polvino SM, et al. (2011) Nanoscale silicon-on-insulator deformation induced by stressed liner structures. *J Appl Phys* 109: 083543.
166. Vartaniants IA, Zozulya AV, Mundboth K, et al. (2008) Crystal truncation planes revealed by three-dimensional reconstruction of reciprocal space. *Phys Rev B* 77: 115317.
167. Yefanov OM, Zozulya AV, Vartaniants IA, et al. (2009) Coherent diffraction tomography of nanoislands from grazing-incidence small-angle x-ray scattering. *Appl Phys Lett* 94: 123104.
168. Zozulya AV, Yefanov OM, Vartaniants IA, et al. (2009) Imaging of nanoislands in coherent grazing-incidence small-angle x-ray scattering experiments. *Phys Rev B* 78: 121304R.
169. Nanver LK, Jovanovis V, Biasotto C, et al. (2011) Integration of MOSFETs with SiGe dots as stressor material. *Solid State Electronics* 60: 75–83.
170. Rodrigues MS, Cornelius TW, Scheler T, et al. (2009) In situ observation of the elastic deformation of a single epitaxial SiGe crystal by combining atomic force microscopy and micro x-ray diffraction. *J Appl Phys* 106: 103525.
171. Cornelius TW, Davydok A, Jacques VLR, et al. (2012) In situ three-dimensional reciprocal-space mapping during mechanical deformation. *J Synch Rad* 19: 688–694.
172. Cornelius TW, Mastropietro F, Thomas O, et al. (2013) In situ nanofocused X-ray diffraction combined with scanning probe microscopy, chapter in X-ray diffraction: Structure, Principles and Applications, ed. Shih K, 223–259, Nova Science Publisher.
173. Kang HC, Yan H, Chu YS, et al. (2013). Oxidation of PtNi nanoparticles studied by a scanning X-ray fluorescence microscope with multi-layer Laue lenses. *Nanoscale* 5:7184.
174. Chu YS (2010) Preliminary Design Report for the Hard X-ray (HXN) Nanoprobe Beamline. National Synchrotron Light Source II, Brookhaven National Laboratory, LT-C-XFD-HXN-PDR-001.
175. Nazaretski E, Lauer K, Yan H, et al. (2015). Pushing the limits: an instrument for hard X-ray imaging below 20 nm. *J Synch Rad* 22:336–341.
176. Vogt S, Lanzirotti A (2013) Trends in X-ray Fluorescence Microscopy. *Synchrotron Radiation News* 26: 32–38.
177. Deng J, Vine DJ, Chen S, et al. (2015) Simultaneous cryo X-ray ptychographic and fluorescence microscopy of green algae. *Proc Nat Acad Sci* 112: 2314–2319.
178. Que EL, Bleher R, Duncan FE, et al. (2015) Quantitative mapping of zinc fluxes in the mammalian egg reveals the origin of fertilization-induced zinc sparks. *Nature Chem* 7: 130–139.
179. Davies R, Burghammer M, Riekel C (2009) A combined microRaman and microdiffraction set-up at the European Synchrotron Radiation Facility ID13 beamline. *J Synch Rad* 16: 22–29.
180. Bernal S, Provis JL, Rose V, et al. (2013). High-resolution X-ray diffraction and fluorescence microscopy characterization of alkali-activated slag-metakaolin binders. *J Am Ceramic Soc* 96: 1951–1957.
181. Andrews JC, Weckhuysen BM (2013) Hard X-ray Spectroscopic Nano-Imaging of Hierarchical Functional Materials at Work. *Chem Phys Chem* 14: 3655.
182. Barrea RA, Gore D, Kujala N (2010) Fast-scanning high-flux microprobe for biological X-ray fluorescence microscopy and microXAS. *J Synch Rad* 17: 522–529.

183. Mocuta C, Richard MI, Fouet J, et al. (2013B) Fast pole figure acquisition using area detectors at DiffAbs beamline – Synchrotron SOLEIL. *J Appl Cryst* 46: 1842–4853.
184. Eriksson M, van der Veen JF, guest editors (2014) Special issue on Diffraction-Limited Storage Rings and New Science Opportunities. J Synch Rad 21: Part 5.
185. Hettel R (2014) Diffraction-limited storage rings DLSR design and plans : an international overview diffraction-limited storage rings. *J Synch Rad* 21:843–855.
186. Mimura H, Handa S, Kimura T, et al. (2010) Breaking the 10 nm barrier in hard-X-ray focusing. *Nature Physics* 6:122–125.
187. Yamauchi K, Mimura H, Kimura T, et al. (2011) Single-nanometer focusing of hard x-rays by Kirkpatrick – Baez mirrors. *J Phys: Condensed Matter* 23:394206.
188. Yan H, Conley R, Bouet N, et al. (2014) Hard x-ray nanofocusing by multilayer Laue lenses. *J Phys D: Appl Phys* 47: 263001.
189. Döring F, Robisch L, Eberl C, et al. (2013) Sub-5 nm hard x-ray point focusing by a combined Kirkpatrick-Baez mirror and multilayer zone plate. *Opt Express* 21: 19311–19323.
190. Mohacsi I, Vartiainen I, Guizar-Sicairos M, et al. (2015) High resolution double-sided diffractive optics for hard X-ray microscopy. *Opt Express* 23:776–786.
191. Schroer CG, Falkenberg G (2014) Hard X-ray nanofocusing at low-emittance synchrotron radiation sources. *J Sync Rad* 21:996–1005.
192. Thibault P, Guizar-Sicairos M, Menzel A (2014) Coherent imaging at the diffraction limit. *J Synch Rad* 21: 1011–1018.
193. Schlichting I, White WE, Yabashi M, guest editors (2015) Special issue on X-ray Free-Electron Lasers, Guest Editors: J Synch Rad 22:Part 3.
194. Solé VA, Papillon E, Cotte M, et al. (25007) A multiplatform code for the analysis of energy-dispersive X-ray fluorescence spectra. *Spectrochim Acta B* 62: 63–68.
195. Ashiotis G, Deschildre A, Nawaz Z, et al. (2015) The fast azimuthal integration Python library: pyFAI. *J Appl Cryst* 48: 510–519.